JPn Neuroscience

The Journal of Physiology

J Physiol 590.19 (2012) pp 4819–4838

Postnatal development of electrophysiological properties of principal neurons in the rat basolateral amygdala

D. E. Ehrlich, S. J. Ryan and D. G. Rainnie

Emory University School of Medicine, Department of Psychiatry and Behavioral Sciences, Division of Behavioral Neuroscience and Psychiatric Disorders, Yerkes Research Center, Atlanta, GA, USA

Key points

- The amygdala mediates emotional processing, in particular fear learning, and disruption of its function is thought to contribute to the developmental origins of psychiatric disorders like depression, anxiety and autism spectrum disorders.
- It is difficult to identify the causes of these disorders or provide effective intervention because most of what is known of amygdala physiology is based on the adult.
- Using the whole-cell patch clamp technique, we show that neurons in the developing rat amygdala undergo drastic changes to their electrophysiology, including passive membrane properties, intrinsic currents and resonance.
- This provides the first evidence that amygdala neuron physiology is dynamic before adulthood, and likely to contribute to emotional development.
- The results help us better understand the normative development of emotional processing and identify critical periods of maturation that may be sensitive to insult.

Abstract The basolateral amygdala (BLA) is critically involved in the pathophysiology of psychiatric disorders, which often emerge during brain development. Several studies have characterized postnatal changes to the morphology and biochemistry of BLA neurons, and many more have identified sensitive periods of emotional maturation. However, it is impossible to determine how BLA development contributes to emotional development or the aetiology of psychiatric disorders because no study has characterized the physiological maturation of BLA neurons. We addressed this critical knowledge gap for the first time using whole-cell patch clamp recording in rat BLA principal neurons to measure electrophysiological properties at postnatal day (P)7, P10, P14, P21, P28 and after P35. We show that intrinsic properties of these neurons undergo significant transitions before P21 and reach maturity around P28. Specifically, we observed significant reductions in input resistance and membrane time constant of nearly 10- and 4-fold, respectively, from P7 to P28. The frequency selectivity of these neurons to input also changed significantly, with peak resonance frequency increasing from 1.0 Hz at P7 to 5.7 Hz at P28. In the same period, maximal firing frequency significantly increased and doublets and triplets of action potentials emerged. Concomitantly, individual action potentials became significantly faster, firing threshold hyperpolarized 6.7 mV, the medium AHP became faster and shallower, and a fast AHP emerged. These results demonstrate neurons of the BLA undergo vast change

D. E. Ehrlich and S. J. Ryan contributed equally to this work.

DOI: 10.1113/jphysiol.2012.237453

throughout postnatal development, and studies of emotional development and treatments for juvenile psychiatric disorders should consider the dynamic physiology of the immature BLA.

(Received 25 May 2012; accepted after revision 24 July 2012; first published online 30 July 2012)
Corresponding author D. Rainnie: Emory University School of Medicine, Department of Psychiatry and Behavioral Sciences, Division of Behavioral Neuroscience and Psychiatric Disorders, Yerkes Research Center, Atlanta, GA, USA. Email: drainni@emory.edu

Abbreviations AHP, afterhyperpolarization; BLA, basolateral amygdala; DC, direct current; fAHP, fast AHP; ISI, inter-spike interval; mAHP, medium AHP; MPO, membrane potential oscillation; R_{in}, input resistance; τ_{memb}, membrane time constant.

Introduction

The basolateral nucleus of the amygdala (BLA) is a major site of sensory input into the amygdala (McDonald, 1998), and activity in this region plays a critical role in regulating emotional behaviour (Davis *et al.* 2003; LeDoux, 2007; Pape & Pare, 2010). A growing body of evidence from basic and clinical research suggests that aberrant activity of the BLA also plays a major role in the aetiology of several psychiatric and neurological disorders, including anxiety, depression, autism and addiction (Adolphs *et al.* 2002; Rainnie *et al.* 2004; Shekhar *et al.* 2005; Truitt *et al.* 2007; Koob & Volkow, 2010). These disorders are commonly expressed early in life (Pine *et al.* 1998; Kim-Cohen *et al.* 2003; McEwen, 2003; Steinberg, 2005), and a wealth of evidence implicates adverse early-life experience as a predisposing factor for psychiatric illness and associated amygdala dysfunction later in life (Heim & Nemeroff, 2002; Zhang *et al.* 2004; Kraszpulski *et al.* 2006; Seidel *et al.* 2008; Hicks *et al.* 2009; Sadler *et al.* 2011). The mechanisms by which early-life experiences impact the developing amygdala remain largely unknown because our understanding of amygdala physiology is based almost exclusively on research conducted in adult animals. Consequently, to better understand how early-life events can impact affective behaviour later in life, a critical first step is to chart the normative developmental trajectory of the amygdala. Here we provide the first evidence for electrophysiological changes in the developing amygdala.

The few studies that have addressed other aspects of amygdala development reveal a highly dynamic neuronal environment in juvenile rodents, which does not begin to stabilize until at least postnatal day (P)28 (Morys *et al.* 1998; Berdel & Morys, 2000; Brummelte *et al.* 2007; Davila *et al.* 2008). For example, the neuronal composition of the BLA is highly dynamic during the first postnatal month. Numerous in the BLA from birth, principal neurons account for about 85% of all neurons in the adult BLA (McDonald, 1985; McDonald *et al.* 1989; Berdel *et al.* 1997*a*). In contrast, interneurons expressing parvalbumin, which comprise a large portion of interneurons, first appear in the BLA around P14 and do not reach mature levels until about P25–30 (Berdel & Morys, 2000). In parallel with these changes, the number of synaptic contacts in the BLA nearly triples, while cell soma size doubles, and neuronal density is halved between P7 and P14 (Berdel *et al.* 1997*a*; Morys *et al.* 1998). These changes are, in turn, mirrored by changes in thalamic and cortical inputs, which only emerge at P7 and are continually refined until P26 (Bouwmeester *et al.* 2002). Finally, the protein expression of key ion channels in BLA neurons changes on a similar time scale (Vacher *et al.* 2006).

We and others have shown that the normal function of the adult BLA is tightly regulated by a reciprocal interaction between principal neurons and GABAergic interneurons (Rainnie *et al.* 1991*a*,*b*; Ehrlich *et al.* 2009; Ryan *et al.* 2012). Given the studies outlined above, the neural circuitry of the BLA, and hence its function, would be predicted to change dramatically across development. Consistent with this premise, at P7 rats approach an aversively-conditioned stimulus, only expressing the mature avoidance behaviour after P10 (Sullivan *et al.* 2000). Similarly, adult-like expression of fear-potentiated startle does not emerge until P23 (Hunt *et al.* 1994; Richardson *et al.* 2000). Other aspects of conditioned fear, including the emergence of trace conditioning and reinstatement, change on a similar time scale (Campbell & Ampuero, 1985; Moye & Rudy, 1987; Kim & Richardson, 2007).

Despite the compelling evidence of early-life transitions in BLA function, no study to date has examined how changes in the physiological properties of individual BLA neurons contribute to these critical periods of development. This information is essential if we are to understand how the adult BLA becomes organized, how it comes to communicate with other brain regions, and how early-life perturbations could influence mature BLA function. We have begun to address this knowledge gap using whole-cell patch clamp recording to characterize the physiological development of BLA principal neurons during the first postnatal month. We show that these neurons undergo significant transitions in intrinsic properties which define their sensitivity to input and characteristic activity, including passive and oscillatory membrane properties, action potential waveform, and spike-train characteristics.

Methods

Ethical approval

All experimental protocols strictly conform to National Institutes of Health guidelines for the Care and Use of Laboratory Animals, and were approved by the Institutional Animal Care and Use Committee of Emory University.

Animals

Rats born in-house to time-mated Sprague–Dawley female rats (embryonic day 14 on arrival, Charles River, Wilmington, MA, USA) were used in all experiments. Pups were housed with the dam prior to weaning on postnatal day (P)22 or P23 (considering P1 as day of birth). After weaning, rats were isolated by sex and housed three to four per cage with access to food and water *ad libitum*. Animals attributed to each recording day (P7, P10, P14, P21 and P28) were recorded on that day or the following day (P7–8, P10–11, P14–15, P21–22 and P28–29, respectively).

Slice preparation

Slices containing the BLA were obtained as previously described (Rainnie, 1999). Briefly, animals were decapitated under isoflurane anaesthesia (Fisher Scientific, Hanoverpark, IL, USA) if older than 11 days, and the brains rapidly removed and immersed in ice cold, 95% oxygen–5% carbon dioxide-perfused 'cutting solution' with the following composition (in mM): NaCl (130), $NaHCO_3$ (30), KCl (3.50), KH_2PO4 (1.10), $MgCl_2$ (6.0), $CaCl_2$ (1.0), glucose (10), ascorbate (0.4), thiourea (0.8), sodium pyruvate (2.0) and kynurenic acid (2.0). Coronal slices containing the BLA were cut at a thickness of 300–350 μm using a Leica VTS-1000 vibrating blade microtome (Leica Microsystems Inc., Bannockburn, IL, USA). Slices were kept in oxygenated cutting solution at 32°C for 1 h before transferring to regular artificial cerebrospinal fluid (ACSF) containing (in mM): NaCl (130), $NaHCO_3$ (30), KCl (3.50), KH_2PO_4 (1.10), $MgCl_2$ (1.30), $CaCl_2$ (2.50), glucose (10), ascorbate (0.4), thiourea (0.8) and sodium pyruvate (2.0).

Patch clamp recording

Individual slices were transferred to a recording chamber mounted on the fixed stage of a Leica DMLFS microscope (Leica Microsystems Inc., Bannockburn, IL, USA) and maintained fully submerged and continuously perfused with oxygenated 32°C ACSF at a flow rate of 1–2 ml min^{-1}. The BLA was identified under ×10 magnification. Individual BLA neurons were identified at ×40 using differential interference contrast (DIC) optics and infrared (IR) illumination with an IR sensitive CCD camera (Orca ER, Hamamatsu, Tokyo Japan). A subset of neurons was filled using patch solution with added biocytin (0.3%) to confirm localization within the BLA. After some recordings, cytosol was recovered and screened using single-cell reverse-transcriptase PCR (as we described previously in Hazra *et al.* 2011) to confirm the presence of the glutamate transporter, VGluT, which was seen in 58/60 neurons tested across all ages. Patch pipettes were pulled from borosilicate glass and had a resistance of 4–6 MΩ. Patch electrode solution had the following composition (in mM): potassium gluconate (130), KCl (2), HEPES (10), $MgCl_2$ (3), K-ATP (2), Na-GTP (0.2) and phosphocreatine (5), titrated to pH 7.3 with KOH, and 290 mosmol L^{-1}. Data acquisition was performed using either a MultiClamp 700A or an Axopatch 1D amplifier in conjunction with pCLAMP 10.2 software and a DigiData 1322A AD/DA interface (Molecular Devices, Sunnyvale, CA, USA). Whole-cell patch clamp recordings were obtained and low-pass filtered at 2 kHz and digitized at 10 kHz. The membrane potential was held at −60 mV for all neurons if not specified. Cells were excluded if they did not meet the following criteria: a stable resting membrane potential more negative than −55 mV; access resistance lower than 30 MΩ; stable access resistance throughout recording, changing less than 15%; and action potentials crossing 0 mV. Where indicated, Cs^+ (5 mM, Sigma-Aldrich, St Louis, MO, USA) was administered by bath application.

Data analysis

Data were analysed by importing the raw voltage and current traces into Matlab (The MathWorks, Natick, MA, USA) using scripts provided with sigTOOL (http://sigtool.sourceforge.net/, developed at King's College London) and processed with customized scripts (available upon request). To characterize neurons in current clamp, first, a series of 10 hyperpolarizing and depolarizing, 1 s long, square-wave current steps were injected. They were scaled so that, for each cell, the peak voltage deflections were to approximately −80 mV and −40 mV (amplitude of negative current injections ranged from a minimum of −20 pA at P7 to a maximum of −1000 pA at P28, and positive current injections from +16 pA at P7 to +800 pA at P28). Second, linear ramps of depolarizing current were injected, lasting 250 ms and scaled to depolarize the neuron to −35 mV and elicit an action potential within the final 50 ms (peak current ranged from a minimum of +85 pA at P7 to a maximum of 555 pA at P28).

Membrane properties and intrinsic currents

Input resistance and time constant were calculated using the deflection (approx. 5 mV) in response to the smallest

hyperpolarizing current step (minimum of −4 pA at P7, maximum of −200 pA at P28). The time constant was defined as the time necessary for the cell to reach 63.2% of its maximal deflection; input resistance was calculated as the ratio of peak voltage deflection to the current injected. To measure the hyperpolarization-activated, non-specific cation current, I_h, neurons were voltage clamped at a holding potential of −60 mV and stepped to −100 mV for 600 ms in the presence of 1 μM TTX. The waveform of the I_h current was generated by subtracting a current trace measured in the presence of bath-applied, 5 mM Cs^+, known to block I_h, from that measured in its absence. This subtraction current was used to measure amplitude and activation time constants of I_h. A two-term exponential fit (eqn (1), $k = 2$) was used to extract fast and slow time constants of I_h activation, except at P7, where two terms over-parameterized the fit and a one-term exponential (eqn (1), $k = 1$) was used instead.

$$f(t) = \sum_{i=1}^{k} A_i \times e^{-t/\tau_i} + C \quad (1)$$

Action potentials and spike trains

Action potentials were detected using a heuristic to locate peaks in the second derivative of the membrane potential waveform. The time of the peak was assigned to be the time of spike initiation and the voltage assigned as action potential threshold, which correlated well with visual inspection of the data. Since the sampling rate used here was not fast compared to the frequency of the action potential waveform (10 kHz compared to ∼1 kHz), linear interpolation between data points was used to enhance the temporal resolution of measurements of 10–90% rise time, 90–10% decay time and half-maximal width. These parameters and average action potential waveforms were calculated using spikes collected in the ramp protocol described above. Fast and medium afterhyperpolarizations (AHPs) were measured on spike-triggered averages from every spike captured (at least 8) during a 1 min recording from neurons clamped manually at action potential threshold with direct current (DC). Fast AHP peak was measured at a local minimum directly following spike repolarization, if visibly distinct from the medium AHP and occurring within 15 ms of spike initiation. Medium AHP peak was measured at the minimum voltage following the spike, if a peak occurred within 150 ms of spike initiation (Storm, 1989).

Data on spike trains were collected from responses to the depolarizing, 1 s-long, square-wave current injections described above. Spike trains were included in the analysis if the mean of their inter-spike membrane potential fell within 1 standard deviation of the spike threshold measured for each age. Inter-spike intervals (ISIs) were calculated using the times for spike initiation in these traces, and the instantaneous firing frequency of the spike train was calculated as the reciprocal of these ISIs.

Resonance and oscillations

Resonance was assessed by injecting neurons with a ZAP current, a sinusoidal current of fixed amplitude that sweeps logarithmically from 0.1 to 12 Hz over 30 s. The amplitude of the current was adjusted to elicit a 20 mV maximal depolarization from a baseline potential of −70 mV. Impedance was calculated as a function of input frequency for each neuron by deriving a power spectrum for the voltage response to the ZAP current, using fast Fourier transforms in the Chronux toolbox for Matlab (Bokil *et al.* 2010), and normalizing it to the power spectrum of the injected current. In order to extract peak values from noisy power spectra and generate averages, the raw impedance traces were fit with a sixth order polynomial. Prominence was calculated using power spectra as the proportion of total power in the entire range considered (1–10 Hz) found in a given frequency band (1–2, 2–4, 4–6, 6–8, or 8–10 Hz). The change in prominence due to Cs^+ application was calculated as a ratio of the power in a given frequency band in Cs^+ and TTX to that in TTX alone. Correlation analysis of the relationship between membrane time constant (τ_{memb}) and peak resonance frequency was performed using GraphPad Prism 4 (GraphPad Software Inc., La Jolla, CA, USA). The presence of membrane potential oscillations (MPOs) in recordings of neurons gradually depolarized to action potential threshold was assessed by an observer blinded to age group. Spike-triggered averages of these depolarized traces were generated using Matlab to observe phase relationships between action potentials and putative MPOs.

Statistics

Data points greater than 2 standard deviations from the mean were deemed outliers and removed from statistical analysis. All data sets were tested for normality using the Shapiro–Wilk test ($\alpha = 0.05$) and for homoscedasticity using Levene's test ($\alpha = 0.0001$), implemented in Matlab. Data sets for mAHP and fAHP amplitude, maximal firing rate, peak resonance frequency, and I_h amplitude passed the Shapiro–Wilk and Levene's tests, so one-way ANOVA with Tukey's *post hoc* test ($\alpha = 0.05$) was used to assess significance. To account for age-dependent changes in variance, values of R_{in}, τ_{memb}, and action potential rise and decay times were log-transformed before statistical analysis. Because the data sets for 6 of 7 basic electrophysiological parameters (R_{in}, τ_{memb}, action potential

half-width, rise time, decay time and first inter-spike interval, but not action potential threshold) failed either the Shapiro–Wilk or Levene's test, all of these data sets were analysed using the Kruskal–Wallis test for overall effect of age on each parameter ($\alpha = 0.05$). The Kruskal–Wallis test was also used for mAHP and fAHP times-to-peak. When a main effect was found, pairwise comparisons were made for each age group with two nearest older and younger groups (i.e. P21 *vs.* P10, 14, 28 and >35) using Wilcoxon's rank sum test (Matlab) with a Bonferroni correction for the resulting nine comparisons ($\alpha = 0.0056$). Significant changes in prominence were assessed using a two-way, repeated measures ANOVA with Bonferroni *post hoc* test, with frequency band as a within-subjects factor and age as a between-subjects factor. Peak resonance frequency was exponentially correlated with τ_{memb} using a least-squares method with eqn (1) ($k = 1$) in GraphPad Prism for all data from P14, P21 and P28.

An analysis of the effects of sex on physiological maturation was performed using a two-way ANOVA with factors of sex and age for the following parameters using GraphPad Prism: R_{in}, τ_{memb}, action potential threshold, half-width, rise time, decay time, and first interspike interval. Significance was assessed for a main effect of sex in each parameter ($\alpha = 0.05$). This analysis included 16 male and female neurons from five male and three female rats at P14, 12 male and female neurons from three male and two female rats at P21, and 12 male and eight female neurons from four male and two female rats at P28. No neurons were included from P7 or P10 due to difficulty assessing sex in the young rats. A *post hoc* power analysis for the effect of sex was conducted using G*Power (Erdfelder *et al.* 1996) with $\alpha = 0.05$.

Results

Data were collected from a total of 499 BLA neurons from 93 rats on postnatal day (P)7, P10, P14, P21 and P28. Also included were data from 53 neurons from 26 older animals ($P > 35$) for comparison with the preadolescent data. To make gross comparisons of neural properties across development, we first examined the voltage response of patch clamped principal neurons to transient (1 s) hyperpolarizing and depolarizing current injections at P7, P14, P21 and P28. As illustrated in Fig. 1, BLA principal neurons at each developmental time point had distinct voltage responses to DC injection. The most obvious changes were to input resistance (R_{in}), membrane time constant (τ_{memb}), the depolarizing voltage sag upon membrane potential hyperpolarization likely to be caused by I_h, and the pattern of action potentials. Below we quantify these and many other physiological changes to BLA principal neurons across the first postnatal month.

Postnatal maturation of passive membrane properties

We measured the passive electrical properties of principal neurons at all time points when manually held at −60 mV with DC injection. Here, R_{in} and τ_{memb} were estimated from small, <5 mV hyperpolarizing voltage deflections elicited by transient current injection. We observed a significant reduction in R_{in} of nearly 10-fold across the first postnatal month (Fig. 2*A*; $P < 0.001$, Kruskal–Wallis, $\chi^2_5 = 241.8$), with the greatest changes occurring before P21. There was a more than twofold reduction in R_{in} from P7 to P14, and a nearly threefold reduction from P14 to P21. Specifically, R_{in} decreased significantly from a median value of 523.7 MΩ at P7 ($n = 45$) to 374.8 MΩ at P10 ($n = 37$), 238.4 MΩ at P14 ($n = 54$), 88.0 MΩ at P21 ($n = 43$) and 55.9 MΩ at P28 ($n = 58$; Wilcoxon's rank sum *post hoc* test). By P28, R_{in} had achieved its mature value and was not significantly different ($P > 0.05$) from neurons aged >P35 (52.67 MΩ, $n = 56$). Membrane time constant followed a similar developmental trajectory to R_{in} (Fig. 2*B* and *C*), with a nearly fourfold reduction from P7 to P28. Overall there was a significant effect of age (Kruskal–Wallis, $\chi^2_5 = 221.4$), with a nearly twofold reduction from P7 to P14 and another twofold decrease from P14 to P28. Whereas the change from P7 to P10 was not significant ($P > 0.05$, Wilcoxon's rank sum *post hoc* test;

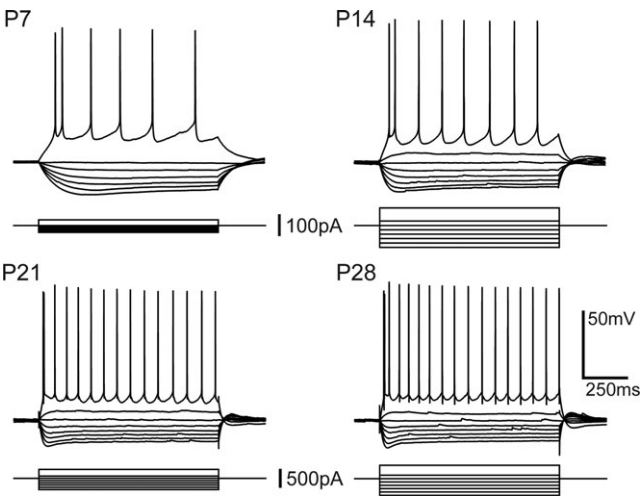

Figure 1. Maturation of physiological properties of BLA principal neurons across the first postnatal month
Illustrated are representative voltage responses to a series of transient (1 s) hyperpolarizing and depolarizing current steps, depicting age-dependent changes in the active and passive membrane properties of BLA principal neurons. All neurons were held at −60 mV with direct current injection. The amplitudes of current injection were adjusted for each neuron to normalize the voltage deflections. Note the difference in scale for the current injections of the neurons depicted in the top panel (postnatal day 7 (P7, left) and 14 (right)) and those depicted in the bottom panel (P21 (left) and 28 (right)).

median = 59.1 ms at P7, $n = 45$; 50.5 ms at P10, $n = 39$), there was a significant ($P < 0.001$) decrease from P10 to P14 (32.0 ms, $n = 53$), P14 to P21 (18.0 ms, $n = 45$), and P21 to P28 (15.1 ms, $n = 56$). Similar to R_{in}, τ_{memb} reached its mature value by P28 and did not change significantly between P28 and >P35 (15.1 ms, $n = 54$; $P > 0.05$). Having observed significant age-dependent changes in the passive membrane properties of BLA principal neurons, we next examined concomitant changes in active properties, beginning with the voltage-gated current, I_h.

Postnatal maturation of intrinsic currents

Development of the voltage-gated current, I_h. One current which classically contributes to passive membrane properties like R_{in} and τ_{memb} is the hyperpolarization-activated cation current, I_h. This current mediates a depolarizing voltage sag observed in response to hyperpolarization from rest that is readily apparent at all ages (Fig. 1). When neurons were manually held at −60 mV and the amplitude of the transient hyperpolarizing current steps adjusted to elicit peak voltage deflections to −80 mV, the depolarizing sags observed in the voltage response had a similar amplitude at all time points (Fig. 3*A*); however, the rate of onset of the sag increased with age. Significantly, the voltage sag was abolished at all ages by bath application of 5 mM Cs^+, suggesting it is likely to be mediated by activation of I_h. An example of the Cs^+ blockade of the depolarizing sag at P28 is illustrated in Fig. 3*A*, upper trace. Considering the differences in R_{in} across ages and the visible differences in the kinetics of the voltage sag, we next quantified the maturation of I_h in voltage clamp.

To quantify the amplitude and kinetics of I_h activation, the membrane potential was stepped from −60 to −100 mV, both before and after application of 5 mM Cs^+, and the resulting currents were then subtracted to isolate I_h. The mean isolated I_h for each time point is illustrated in Fig. 3*B*. Analysis of the peak amplitude revealed a steady increase of I_h amplitude across the entire first postnatal month (Fig. 3*C*), such that the mean I_h amplitude was 91.5 ± 28.1 pA at P7 ($n = 10$), 359.8 ± 82.3 pA at P14 ($n = 14$), 518.1 ± 239.2 pA at P21 ($n = 11$), and 641.9 ± 239.8 pA at P28 ($n = 11$). Notably, significant transitions occurred from P7 to P14 and from P14 to P28 ($P < 0.01$, one-way ANOVA with Tukey's *post hoc* test, $F_{3,42} = 19.93$). The activation kinetics of I_h were estimated by fitting its charging curve with a two-term exponential equation, except at P7, when the curve was sufficiently parameterized with a one-term exponential. The fast time constant decreased from 25.4 ± 6.3 ms at P14 ($n = 19$) to 19.6 ± 2.4 ms at P21 ($n = 15$), but remained steady between P21 and P28 (19.1 ± 2.7 ms, $n = 13$; Fig. 3*D*, filled circles). The single time constant at P7 was 188.5 ± 61.1 ms ($n = 11$), which was similar to the slow time constant of activation for the other ages (253.5 ± 65.2 at P14, 252.9 ± 127.7 at P21, and 361.7 ± 340 at P28; Fig. 3*D*, filled triangles).

Development of intrinsic resonance. Membrane properties like τ_{memb} and active currents like I_h help shape intrinsic resonance, which acts as a band-pass filter to enhance responsiveness to synaptic input at particular frequencies. BLA principal neurons in the adult rat, guinea pig and primate exhibit a preferred resonance frequency between 2.5 and 6 Hz (Pape & Driesang, 1998; Ryan *et al.* 2012). Resonance properties of neurons

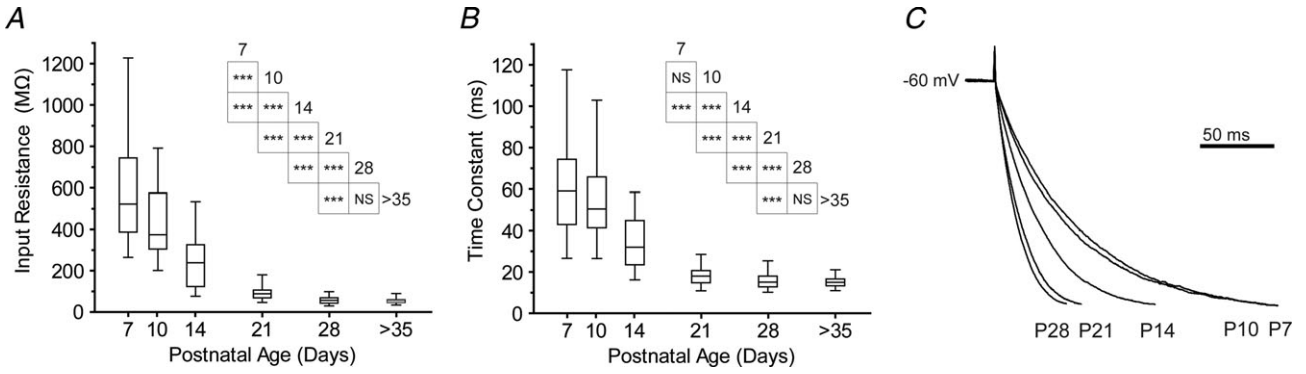

Figure 2. Input resistance and membrane time constant decrease with age
A and *B*, box and whisker plots show input resistance (*A*) and membrane time-constant (*B*) of BLA principal neurons across the first postnatal month and in adulthood ($n = 45$ (P7), 37–39 (P10), 53–54 (P14), 43–45 (P21), 56–58 (P28), and 54–56 ($P > 35$)). Significance was assessed using Wilcoxon's rank-sum test and pairwise comparisons were made for each age group with up to four neighbouring time points (see inset tables for results) using a Bonferroni correction for the resulting 9 comparisons (***$P < 0.001$; NS: not significant, $P > 0.05$). *C*, maturation of membrane time constant is illustrated with the average, normalized membrane charging in response to a small, hyperpolarizing current step (approximately 5 mV deflection) for each developmental time point ($n = 48$ (P7), 28 (P10), 56 (P14), 45 (P21), and 58 (P28)).

are likely to contribute to the production of network oscillations (Lampl & Yarom, 1997; Desmaisons *et al.* 1999; Richardson *et al.* 2003; Tohidi & Nadim, 2009), and recent evidence suggests that network oscillations in the BLA at the frequency of principal neuron resonance are intimately related to fear memory formation and expression (Popa *et al.* 2010; Lesting *et al.* 2011). Considering the potential contribution of BLA principal neuron resonance to the generation of fear expression and learning, we next examined the ontogeny of resonance properties in these neurons.

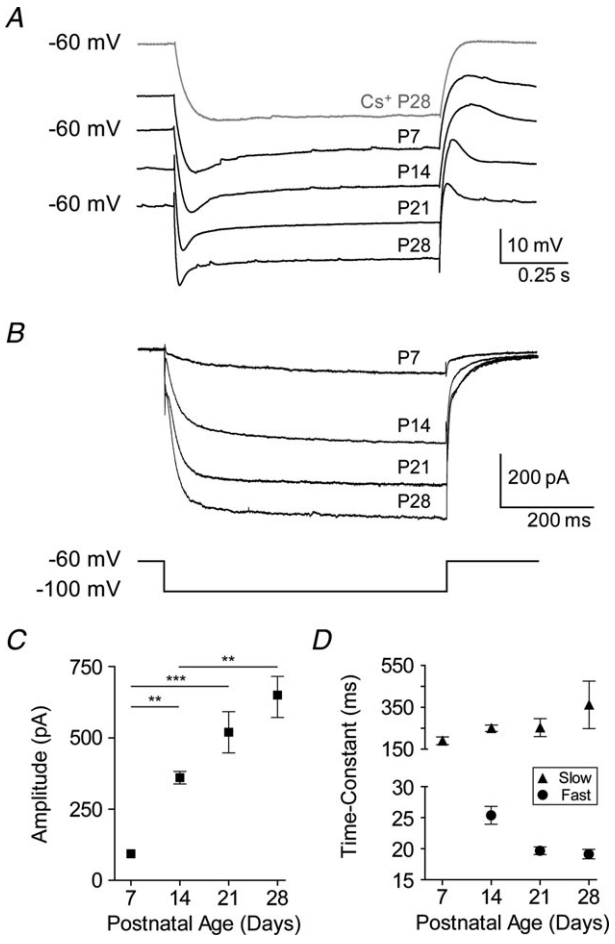

Figure 3. Developmental increase in I_h amplitude and kinetics in BLA principal neurons
A, representative voltage responses of neurons to a hyperpolarizing, square step of magnitude adjusted to elicit a 20 mV peak deflection. Neurons were recorded in the presence of 1 μM TTX at each time point, and blockade of I_h by 5 mM caesium (Cs^+) is depicted for a neuron at P28. Neurons had baseline membrane potential adjusted to −60 mV with direct current. *B*, voltage-clamp recordings following Cs^+ application (5 mM) subtracted from those prior to Cs^+ application depict the maturation of a Cs^+-sensitive current. Neurons were held at −60 mV and stepped to −100 mV, and all recordings were performed in the presence of 1 μM TTX ($n = 10$ (P7), 14 (P14), 11 (P21), 11 (P28)). *C*, peak amplitudes of subtraction currents from *B* are plotted as means ± SEM for each time point. Significance was assessed using a one-way ANOVA with Bonferonni's *post hoc* test, and pairwise comparisons were made for each age group with up to three neighbouring time points (***$P < 0.001$; **$P < 0.01$). *D*, plotted as means ± SEM for each age, the time constant of I_h activation was measured from a double exponential fit to the subtraction currents in *B* at all ages except P7, which was sufficiently fitted with a single exponential.

By injecting a sinusoidal ZAP current of increasing frequency (see Methods) we were able to determine the peak resonance frequency, the input frequency that elicits the greatest membrane deflection, of BLA principal neurons across development. As illustrated in Fig. 4*A*, the population responses to ZAP currents at P7, P14, P21 and P28 clearly showed a shift in the resonance frequency of principal neurons, with more mature neurons showing higher resonance frequencies. By taking the ratio of power spectra for output voltage and ZAP input current, we generated functions of impedance *vs.* input frequency (Fig. 4*B*). Here, the peak resonance frequency increased sharply and significantly until P21 ($P < 0.001$, one-way ANOVA with Tukey's *post hoc* test, $F_{3,91} = 74.31$), with values (mean ± SD) of 0.97 ± 0.33 Hz at P7 ($n = 21$), 2.63 ± 1.48 Hz at P14 ($n = 24$), 5.47 ± 1.30 Hz at P21 ($n = 21$), and 5.69 ± 1.49 Hz at P28 ($n = 29$; Fig. 4*C*).

To determine how developmental changes in I_h may contribute to the maturation of resonance, we blocked I_h using Cs^+ and measured changes in the responses to ZAP currents across the first postnatal month (Fig. 5*A*). At all ages, Cs^+ application reduced the peak resonance frequency to below 1 Hz (0.60 ± 0.09 Hz at P7 ($n = 8$), 0.67 ± 0.22 Hz at P14 ($n = 9$), 0.85 ± 0.29 Hz at P21 ($n = 8$), and 0.94 ± 0.49 Hz at P28 ($n = 11$)). However, the effect of Cs^+ blockade on resonance involves more than a change in peak frequency; therefore, to highlight differences in the contribution of I_h to resonance across ages, we quantified the effect of Cs^+ on prominence, the proportion of total power between 1 and 10 Hz found in a given frequency band (1–2, 2–4, 4–6, 6–8, or 8–10 Hz) (Burton *et al.* 2008).

As shown in Fig. 5*B*, the change in prominence due to Cs^+ application varied by age as an inverted 'U' with Cs^+ having relatively little impact at P7 and causing robust changes at P14, then having a progressively weaker effect at later time points. There were significant main effects on change in prominence of frequency band ($F_{4,272} = 518.1$, $P < 0.0001$, two-way ANOVA with repeated measures) and age ($F_{3,272} = 28.9$, $P < 0.0001$), as well as a significant interaction effect ($F_{12,272} = 40.9$, $P < 0.0001$). Specifically, at P7 Cs^+ increased prominence (mean ± SD) at 1–2 Hz by 32.9 ± 20.1% and reduced prominence in the higher bands by between 3 and 20% each ($n = 18$). Compared to P7, Cs^+ application at P14 caused a significantly greater increase in prominence in the 1–2 and 2–4 Hz bands (+157.3 ± 49.4% and +28.2 ± 12.6%, respectively; $P < 0.001$, Bonferroni *post*

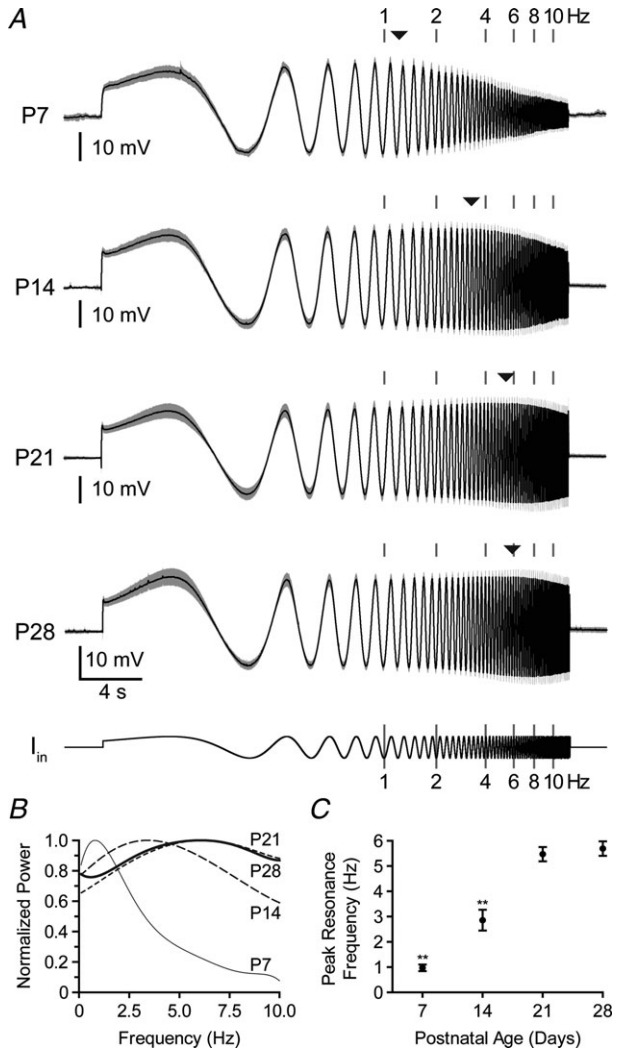

Figure 4. Maturation of intrinsic resonance towards higher frequencies
A, membrane potential response, shown as mean (black line) and standard deviation (grey band), to a ZAP current (I_{in}, fixed amplitude and logarithmically increasing frequency, shown at bottom) is depicted for each age ($n = 22$ (P7), 24 (P14), 22 (P21), and 32 (P28)). Neurons were first hyperpolarized to −70 mV with direct current, and ZAP current amplitude was adjusted for each neuron to elicit a 20 mV depolarizing deflection. Instantaneous frequency of the injected current is highlighted with grey bars above each trace, and the mean, peak resonance frequency for each age is depicted amid the grey bars with a filled triangle. *B*, relative impedance for input from 0.1–10 Hz, calculated by normalizing the power spectra of the voltage responses in *A* to the power spectra of injected current, were fitted with polynomials and plotted as the mean (*n* consistent with *A*). *C*, peak resonance frequency is plotted as means ± SEM, measured at the maximum of each neuron's individual power spectrum ($n = 21$ at P7, 24 at P14, 21 at P21, and 29 at P28). Statistical significance was assessed with a one-way ANOVA using Bonferroni's *post hoc* test to compare all data sets (**$P < 0.001$ *versus* all other groups).

hoc test), and a significantly greater reduction in the 4–6, 6–8 and 8–10 Hz bands (−31.8 ± 7.5%, −53.0 ± 9.0%, and −58.3 ± 7.6%, respectively; $n = 19$; $P < 0.01$). The effect of Cs^+ at P21 was significantly weaker than at P14 ($P < 0.001$) in the 1–2, 4–6 and 6–8 Hz bands and significantly greater ($P < 0.01$) in the 2–4 Hz band (+113.9 ± 43.1% at 1–2 Hz, +44.6 ± 16.3% at 2–4 Hz, −9.5 ± 6.7% at 4–6 Hz, −35.0 ± 9.3% at 6–8 Hz, and −46.5 ± 11.5% at 8–10 Hz; $n = 19$). The trend continued at P28, with Cs^+ having a weaker effect than at P21. Specifically, Cs^+ caused a significantly smaller increase in prominence in the 1–2 Hz band ($P < 0.001$; +68.9 ± 27.4%) but effects in the remaining bands were not significantly different than at P21 (+33.4 ± 13.5% at 2–4 Hz, −2.2 ± 4.3% at 4–6 Hz, −23.7 ± 8.9% at 6–8 Hz, and −34.8 ± 11.8% at 8–10 Hz; $n = 16$).

The effects of Cs^+ on resonance were largely attributable to a direct effect on τ_{memb}. In control conditions, peak resonance frequency was correlated with τ_{memb} using a standard exponential equation (see Methods), yielding a R^2 value of 0.76 with $A_1 = 12.42$, $\tau_1 = 17.24$ and $C = 0.28$ (Fig. 5*C*). Application of Cs^+ increased τ_{memb} at P14, P21 and P28 by an average of 67.0, 19.0 and 24.5 ms, respectively, causing a corresponding reduction in peak resonance frequency at each age (Fig. 5*D*). Based on these observed changes to oscillatory properties of BLA principal neurons, we next characterized the maturation of spontaneous expression of membrane oscillations.

Development of spontaneous membrane potential oscillations. The oscillatory properties of adult BLA principal neurons manifest not only as resonance, but also as spontaneous membrane potential oscillations (MPOs; Pape *et al.* 1998; Ryan *et al.* 2012). These MPOs can influence spike timing and interact with resonance to filter synaptic input based on frequency (Desmaisons *et al.* 1999; Izhikevich, 2002; Sancristobal *et al.* 2010). Furthermore, we have recently shown that phase-locked MPOs and coordinated spiking in adult BLA principal neurons are promoted by spontaneous, synchronous inhibitory postsynaptic potentials, highlighting a mechanism by which MPOs could contribute to network oscillations in the BLA (Ryan *et al.* 2012). We were therefore interested in the ontogeny of network oscillations in the BLA, and next examined the expression of MPOs in neurons at P7, 14, 21 and 28. Here, principal neurons were depolarized to action potential threshold with DC injection. As illustrated in Fig. 6*A*, neurons at P7 were more likely to fire action potentials in bursts, whereas P28 neurons had a more stable membrane potential and fired sporadically (Fig. 6*A*). When depolarized to threshold, neurons also became more likely to exhibit spontaneous MPOs across the first postnatal month (Fig. 6*B* and *C*). A blinded, qualitative analysis of current-clamp recordings

near threshold revealed that only 5% of BLA principal neurons exhibited spontaneous MPOs at P7 ($n = 20$) and P10 ($n = 19$), but MPOs were present in 23% of neurons at P14 ($n = 26$), 64% at P21 ($n = 25$), and 60% at P28 ($n = 48$). Moreover, when we measured the frequency of spontaneous MPOs for neurons with a discernible peak in the power spectrum of their activity during a low-spiking period at threshold, we observed that it increased with development (3.8 ± 1.0 Hz at P14, $n = 3$; 3.7 ± 1.9 Hz at P21, $n = 12$; 4.4 ± 1.9 Hz at P28, $n = 22$). In other brain regions, MPOs are capable of organizing action potential timing (Llinas *et al.* 1991; Gutfreund *et al.* 1995; Desmaisons *et al.* 1999), and the same appears to be true in the BLA. An example of this is illustrated in Fig. 6*D*, which shows a spike-triggered average from a P28 neuron.

Postnatal maturation of spiking

Development of spike trains. Having observed significant developmental changes in the sensitivity of BLA principal neurons to input as well as gross changes in action potential output (see Figs 1 and 6*A*), we next quantified the maturation of action potential trains across the first postnatal month. Here, spike trains were elicited

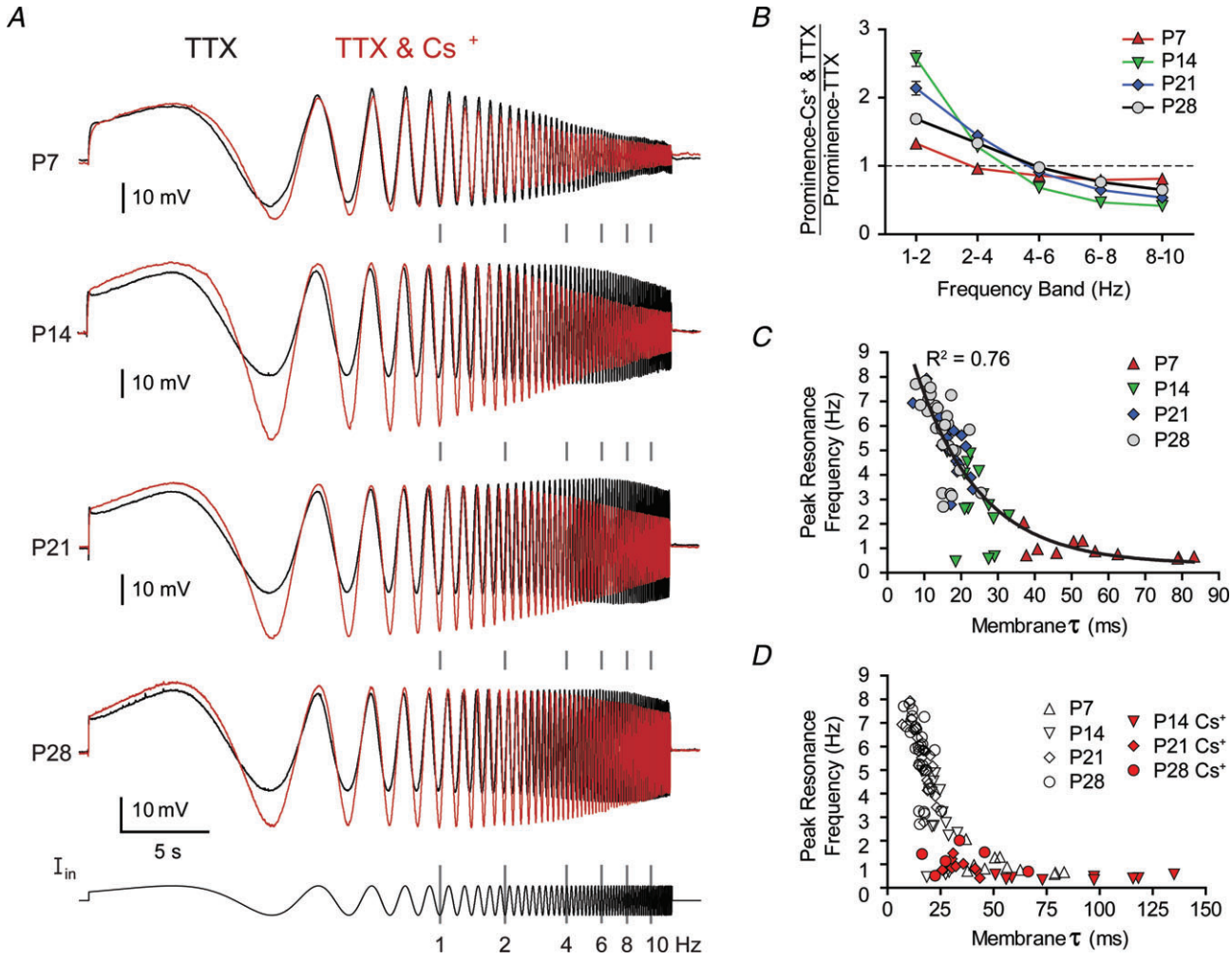

Figure 5. Contribution of I_h to intrinsic resonance of BLA principal neurons changes with age
A, mean membrane potential response to a ZAP current (I_{in}, fixed amplitude and logarithmically increasing frequency, shown at bottom) in 1 μM TTX alone (black line, taken from Fig. 6) or with 5 mM Cs^+ (red line) is depicted for each age (in Cs^+, $n = 19$ at P7, 21 at P14, 20 at P21, and 17 at P28). Neurons were first hyperpolarized to -70 mV with direct current, and ZAP current amplitude was adjusted for each neuron and condition to elicit a 20 mV, maximal depolarizing deflection. Instantaneous frequency of the injected current is highlighted with grey bars between traces. *B*, effect of Cs^+ application on prominence, calculated as ratio of the prominence before and after Cs^+ application, plotted as mean and SEM at P7, P14, P21 and P28. *C* and *D*, peak resonance frequency is plotted against membrane time constant (τ) for neurons at each time point, recorded in TTX alone (*C* and *D*) or following application of 5 mM Cs^+ (*D*). A black line depicts the results of an exponential regression ($R^2 = 0.76$) of the data shown in *C*.

with a transient, 1 s, square-wave depolarizing current injection to action potential threshold. As illustrated in Fig. 7, there was a gradual emergence across the first postnatal month of doublet and triplet firing at the onsets of the spike trains. Moreover, analysis of the instantaneous firing rates based on the first six inter-spike-intervals (ISIs) for principal neurons at P7, 14, 21 and 28 revealed that at P7 the firing rate was relatively consistent across the entire train, starting at 29.7 ± 13.3 Hz and stabilizing at 16.8 ± 8.1 Hz by the third interval (Fig. 7*A*). By P14, doublets became more apparent with an initial firing rate of 62.2 ± 52.1 Hz that dropped to 17.3 ± 12.5 Hz by the second interval. At P21, the doublet became faster and a triplet emerged in some neurons, with firing rates of 138.8 ± 77.9 and 45.0 ± 44.5 Hz for the first and second intervals, respectively, which stabilized around 20 Hz for the remainder of the train. Firing at P28 was very similar to that at P21, with slightly faster rates for the first pair of spikes (166.9 ± 95.3 Hz). We quantified the emergence of doublets using the first ISI, which significantly decreased from P14 to 21 and from P21 to 28 (Fig. 7*B*; $P < 0.001$, Kruskal–Wallis with Wilcoxon's rank sum *post hoc* test, $\chi^2{}_5 = 194.0$). Every transition between neighbouring pairs of time points was significant as well ($P < 0.001$).

We next measured the input–output relationship for action potential generation at P7, 14, 21 and 28 ($n = 7$, all groups), using 1 s, square-wave current injections applied from a resting membrane potential of −60 mV. As illustrated in Fig. 7*C*, as neurons matured they required more current to generate the same output frequency. Interestingly, although the maximal firing frequency (mean ± SD) significantly increased ($P < 0.001$, one-way ANOVA with Tukey's *post hoc* test, $F_{3,23} = 25.96$) from P7 (15.9 ± 3.3 Hz) to P14 (33.9 ± 7.3 Hz), the transitions ($P > 0.05$) from P14 to P21 (34.7 ± 3.7 Hz) and from P21 to P28 (36.5 ± 4.2 Hz) were not significant.

Development of the action potential waveform. We reasoned that the observed changes in spike trains were likely to be due, in part, to maturation of the waveform of individual action potentials. Consequently, to quantify changes in action potential waveform, neurons were probed with a depolarizing current ramp lasting 250 ms, whose amplitude was adjusted to elicit a single action potential. Figure 8*A* illustrates the mean action potential waveforms from each age group. As can be seen, action potential threshold exhibited a significant, negative shift of approximately 7 mV from P7 to P28 (Kruskal–Wallis, $\chi^2_5 = 164.5$, Fig. 8*B*). The median threshold was −33.5 mV at P7 ($n = 51$), −34.7 mV at P10 ($n = 35$), −37.0 mV at P14 ($n = 52$), −40.9 mV at P21 ($n = 43$), −40.3 mV at P28 ($n = 56$), and −41.3 mV at >P35 ($n = 55$). Statistically

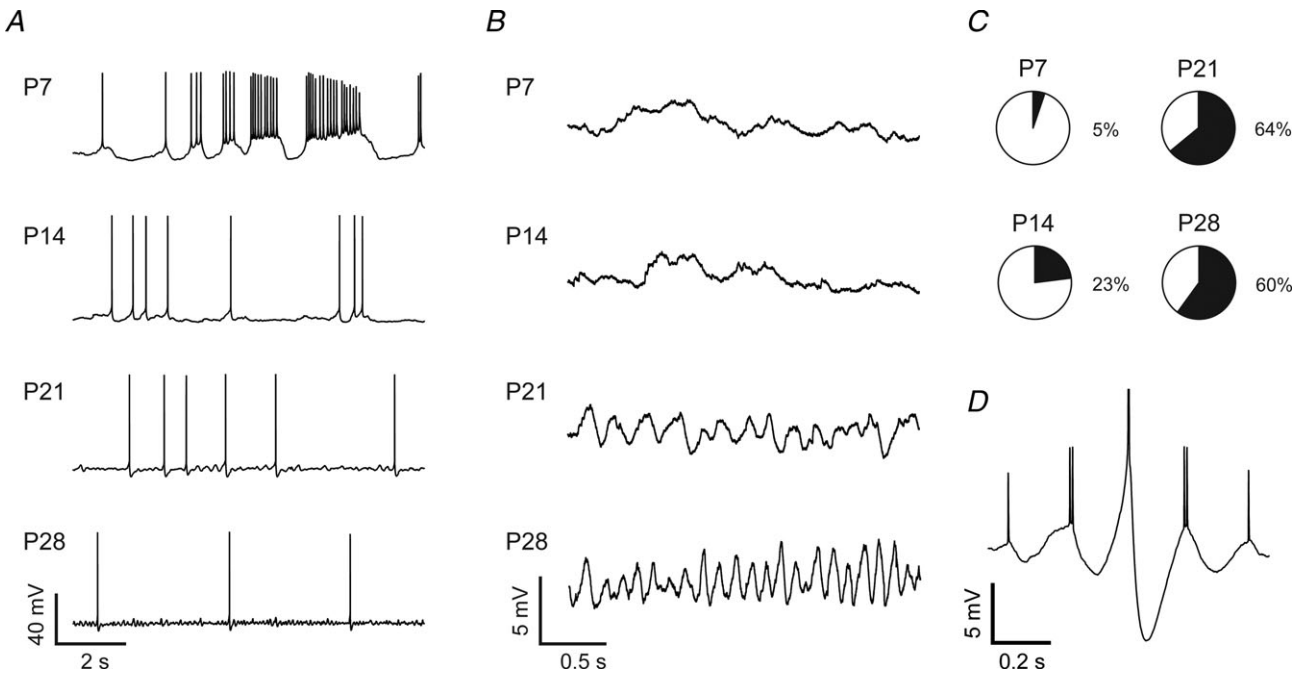

Figure 6. Spontaneous membrane potential oscillations emerge as BLA principal neurons develop
A and *B*, representative current-clamp recordings, shown at two scales, of neurons depolarized to action potential threshold with direct current, highlighting maturation of spiking pattern (*A*) and spontaneous membrane potential oscillations (*B*). *C*, pie charts depict the proportion of neurons expressing spontaneous membrane potential oscillations at each time point ($n = 20$ (P7), 26 (P14), 25 (P21), and 48 (P28)). *D*, representative spike-triggered average from a 30 s recording of a P28 neuron held near threshold, displaying entrainment of spiking to a spontaneous membrane potential oscillation.

significant transitions occurred from P10 to P14 and P14 to P21 ($P < 0.001$, Wilcoxon's rank sum *post hoc* test). In addition, action potentials became much faster; the action potential half-width decreased between P7 and P28 (Fig. 8*C*), with the value at each time point being significantly faster than at the previous ($P < 0.01$, Kruskal–Wallis with Wilcoxon's rank sum *post hoc* test, $\chi^2_5 = 217.8$). The median half-width was 1.39 ms at P7 ($n = 49$), 1.23 ms at P10 ($n = 35$), 1.11 ms at P14 ($n = 52$), 0.90 ms at P21 ($n = 44$), 0.76 ms at P28 ($n = 56$), and 0.83 ms at $P > 35$ ($n = 57$). Action potential 10–90% rise time also decreased over this window, but the change was more gradual (Fig. 8*D*). Here, the median rise time was 0.56 ms at P7 ($n = 51$), 0.47 ms at P10 ($n = 37$), 0.42 ms at P14 ($n = 55$), 0.37 ms at P21 ($n = 45$), 0.30 ms at P28 ($n = 57$), and 0.32 ms at $P > 35$ ($n = 55$). The only significant neighbouring comparison in rise time was between P21 and P28 ($P < 0.001$, Kruskal–Wallis with Wilcoxon's rank sum *post hoc* test, $\chi^2_5 = 134.7$), but every transition across two time points was significant ($P < 0.001$). Finally, the 90–10% decay time also decreased more than twofold from P7 to P28 (Fig. 8*E*) and decreased significantly between every neighbouring pair of time points aside from P10 to 14 ($P < 0.001$, Kruskal–Wallis with Wilcoxon's rank sum *post hoc* test, $\chi^2_5 = 201.6$). Here, the median decay-time was 1.64 ms at P7 ($n = 50$), 1.30 ms at P10 ($n = 36$), 1.07 ms at P14 ($n = 53$), 0.83 ms at P21 ($n = 43$), 0.66 ms at P28 ($n = 56$), and 0.86 ms at $P > 35$ ($n = 56$).

Development of afterhyperpolarization. The maturation of action potential duration strongly suggested that calcium influx due to individual spikes would also change significantly. Hence, we next examined the developmental expression of post-spike afterhyperpolarizations (AHPs), which have been shown to have some calcium dependency in amygdala principal neurons (Faber & Sah, 2002) and could further contribute to the observed changes in spike trains. As expected, AHP expression also matured across the first postnatal month, with clear changes in both the fast and medium AHP (fAHP and mAHP, respectively). Figure 9*A* illustrates representative AHPs of BLA principal neurons at P7, 14, 21 and 28. As can be seen, the mAHP is already present at P7, whereas a distinct fAHP does not appear until P21. As shown in Fig. 9*B*, the mAHP became faster and more shallow from P7 to P28, with times-to-peak of 91.4 ± 11.8 ms at P7

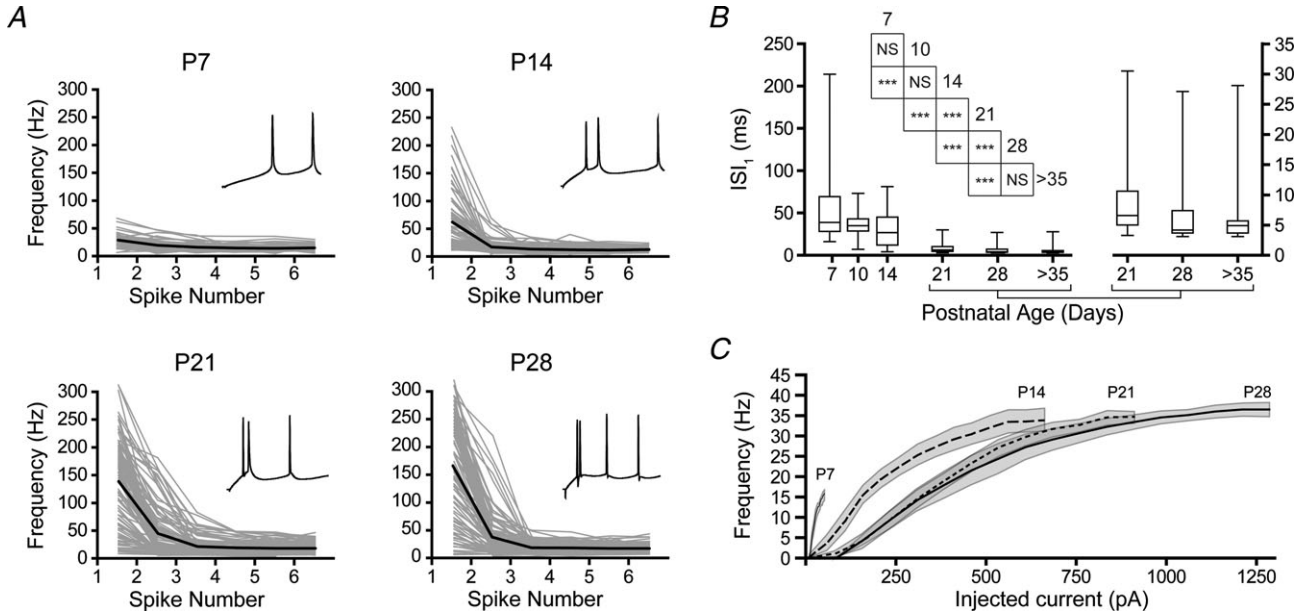

Figure 7. Maturation of spike trains in BLA principal neurons
A, instantaneous action potential frequency is plotted for individual neurons (grey lines) and group mean (black lines) at each time point. Neurons were depolarized such that the mean inter-spike membrane potential was near spike threshold (see Methods for details). The start of a representative spike train is inset in each plot to highlight differences in initial spike rate ($n = 39$ (P7), 75 (P14), 97 (P21), and 103 (P28) trains). *B*, first interspike-interval for the spike trains in *A* is depicted in a box and whisker plot, with the later time points shown on both *y*-axes ($n = 45$ (P7), 37 (P10), 53 (P14), 43 (P21), 54 (P28), and 59 ($P > 35$)). Significance was assessed using Wilcoxon's rank-sum test and pairwise comparisons were made for each age group with up to 4 neighbouring time points (see inset table for results) using a Bonferroni correction for the resulting 9 comparisons (***$P < 0.001$; NS: not significant, $P > 0.05$). *C*, input–output curves for neurons at each time point are depicted as mean (line) and standard deviation (grey band) of average firing frequency in response to a 1 s square current step from holding potential at −60 mV ($n = 7$ for all time points).

($n = 8$), 69.0 ± 5.8 ms at P14 ($n = 15$), 59.8 ± 3.8 ms at P21 ($n = 22$), and 57.2 ± 3.6 ms at P28 ($n = 42$). The amplitude of the mAHP was −14.9 ± 2.4 mV at P7, −13.2 ± 1.9 mV at P14, −12.4 ± 2.6 mV at P21, and −11.1 ± 1.9 mV at P28. There was a significant effect of age on mAHP amplitude ($P < 0.001$, one-way ANOVA, $F_{3,83} = 8.95$) and duration ($P < 0.01$, Kruskal–Wallis, $\chi^2_3 = 11.45$). The fAHP emerged at P14 (Fig. 9*C*), with 33% of neurons exhibiting a fAHP. The proportion increased to 68% by P21 and to 74% by P28. The fAHP became faster across this period, with times-to-peak (mean ± SEM) of 2.8 ± 0.1 ms at P14 ($n = 5$ of 15), 2.4 ± 0.1 ms at P21 ($n = 15$ of 22), and 2.4 ± 0.1 ms at P28 ($n = 31$ of 42). The fAHP also became deeper, with amplitudes (mean ± SD) of −2.8 ± 2.6 mV at P14, −5.2 ± 2.3 mV at P21, and −6.1 ± 3.1 mV at P28. The effect of age was not significant for fAHP amplitude ($P = 0.052$, one-way ANOVA, $F_{2,48} = 3.147$) and duration ($P = 0.061$, Kruskal–Wallis, $\chi^2_2 = 5.61$).

No effect of sex on postnatal changes in physiological properties

Due to differences in emotional processing and development of emotional behaviours across sexes, there is great interest in sex differences in amygdala maturation. Therefore, we performed a statistical analysis to assess sex differences in many of the physiological properties discussed above. Using a two-way ANOVA with factors of age and sex, we compared groups of between 8 and 16 neurons per sex at P14, 21 and 28. We found no main effect of sex ($P > 0.05$) in any of the parameters tested (R_{in}, τ_{memb}, action potential threshold, half-width, 10–90% rise time, 90–10% decay time, and first ISI). We conducted a *post hoc* power analysis using *G*Power* (Erdfelder *et al.* 1996) to assess whether we had sufficient power to detect an effect of sex. The power to detect a large effect size ($f = 0.40$, Cohen, 1977) was 0.94, but the power to detect a medium-sized effect ($f = 0.25$) was 0.59. Therefore, we cannot rule out the possibility of an effect of sex on these

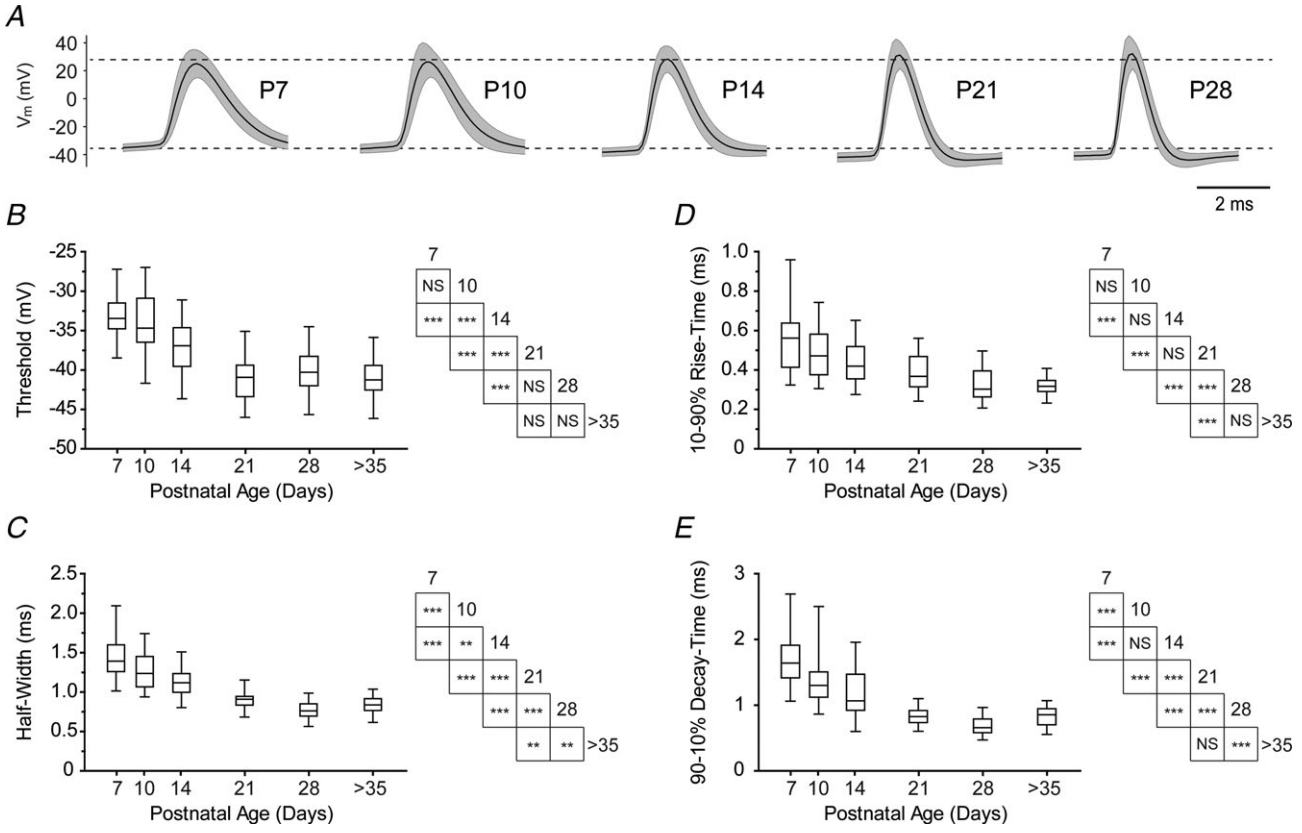

Figure 8. Action potentials of BLA principal neurons develop a more hyperpolarized threshold and become faster with age
A, action potential waveform, depicted as mean (black line) and standard deviation (grey band), for neurons across postnatal development ($n = 48$ (P7), 34 (P10), 46 (P14), 40 (P21), 54 (P28)). *B–E*, box and whisker plots depict action potential threshold (*B*), half-width (*C*), 10–90% rise-time (*D*), and 90–10% decay time (*E*) for neurons at each time point ($n = 49$–51 (P7), $n = 35$–37 (P10), $n = 52$–55 (P14), $n = 43$–45 (P21), $n = 56$–57 (P28), and $n = 55$–57 ($P > 35$)). Significance was assessed using Wilcoxon's rank-sum test and pairwise comparisons were made for each age group with up to four neighbouring time points (see inset tables for results) using a Bonferroni correction for the resulting 9 comparisons (***$P < 0.001$; **$P < 0.01$; NS: not significant, $P > 0.05$).

parameters in development, but expect such an effect would not be large. It is important to note that all measures were taken before sexual maturity, and large effects of sex may emerge by adulthood.

Discussion

In this study, we have provided the first evidence that physiological properties of principal neurons in the rat BLA undergo significant change during the first postnatal month. Characterizing how neurons of the amygdala develop is fundamental to understanding normative emotional development and, in turn, how risk factors and genetic predispositions are translated into developmental emotional disorders like anxiety, depression, autism spectrum disorders, and schizophrenia (Pine, 2002; Kim-Cohen *et al.* 2003; Kessler *et al.* 2005; Monk, 2008). Emotional processing, in particular fear learning, is critically dependent on the BLA (Davis, 2000; LeDoux, 2000), and the rapid and robust changes to fear learning observed during the first postnatal month in rats suggest the BLA develops profoundly during this period (Campbell & Ampuero, 1985; Moye & Rudy, 1987; Hunt *et al.* 1994; Sullivan *et al.* 2000; Kim & Richardson, 2007). To facilitate comparisons of the timing of our observations to milestones in other species, consider that an infant rat first opens its eyes and reaches comparable cortical maturity to a newborn human at around two weeks after birth, is weaned around three, and reaches sexual maturity between six and eight (Quinn, 2005). In our hands, BLA principal neurons exhibited the greatest physiological changes between P7 and P21. Furthermore, neuronal physiology at P28 very closely resembled that of neurons recorded after P35, as well as previous reports of adult BLA principal neurons. These findings suggest that the electrophysiological properties of neurons in the human amygdala may undergo the largest transitions before 1 year of age and continue to develop into early adolescence. All of these changes support the notion that the BLA and its contribution to emotional processing are in flux well into postnatal life, marking a period of vulnerability for the circuit and long-term emotional outcomes (Spear, 2009).

Maturation of passive membrane properties

The most fundamental aspect of physiology in which we observed changes was passive membrane properties. For both input resistance (R_{in}) and membrane time constant

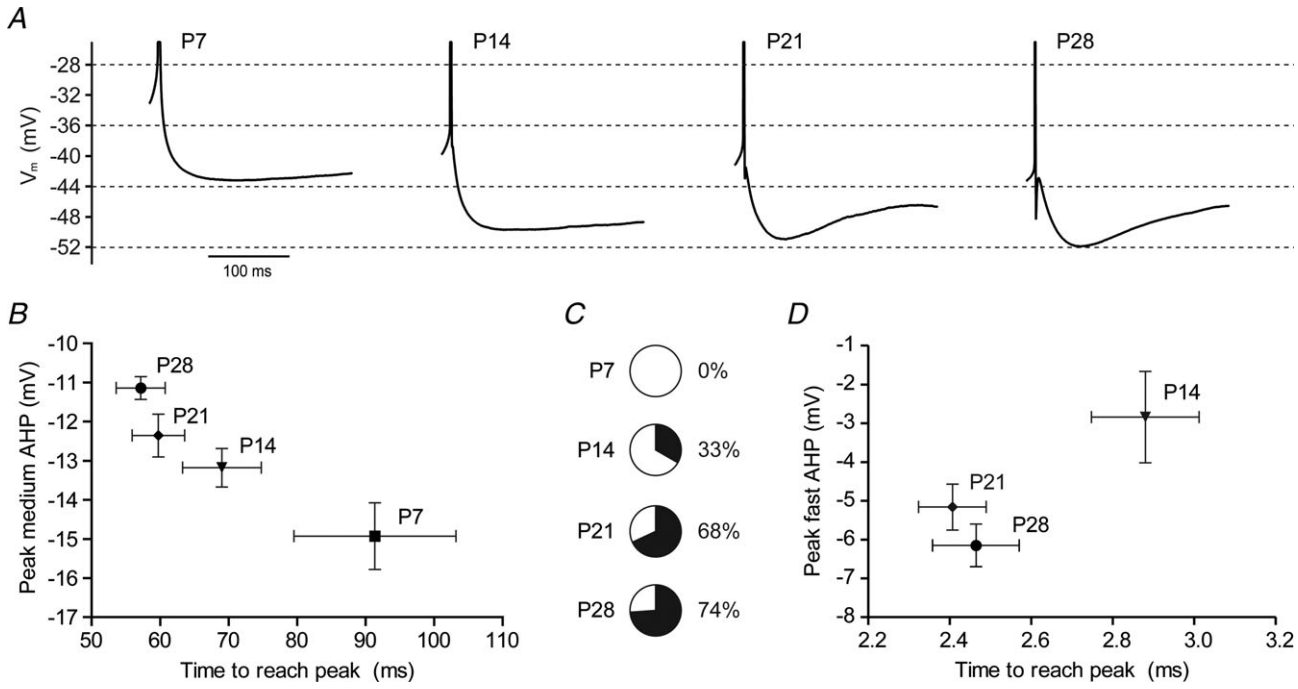

Figure 9. Action potential medium AHP matures and a fast AHP emerges with age
A, changes in afterhyperpolarization (AHP) waveform are illustrated by spike-triggered averages (from at least 8 action potentials) of one free-firing, representative neuron for each time point. *B* and *D*, derived from spike-triggered averages, the voltage difference between a neuron's action potential threshold and its medium (*B*) or fast (*D*) AHP peak (mean ± SEM) is plotted *versus* time elapsed from spike initiation to AHP peak (mean ± SEM) for each time point ($n = 8$ (P7), 15 (P14), 22 (P21), and 31 (P28)). There was a significant effect of age on mAHP amplitude ($P < 0.001$, one-way ANOVA) and duration ($P < 0.01$, Kruskal–Wallis). Only neurons with a discernible fast AHP were included in analysis for *D*, and the proportions of neurons expressing a fast AHP at each time point are depicted as pie charts (*C*).

(τ_{memb}), a great proportion of maturation took place by P21. In fact, R_{in} decreased sixfold and τ_{memb} more than threefold between P7 and P21. The values we report for R_{in} and τ_{memb} at P28 and >P35 match those reported previously for adult BLA principal neurons (Rainnie *et al.* 1993), suggesting these neurons are physiologically mature by P28. These trajectories are also comparable to those seen in sensorimotor (McCormick & Prince, 1987) and prefrontal cortex (Zhang, 2004) as well as thalamus (Ramoa & McCormick, 1994). The decreases in R_{in} and τ_{memb} are consistent with the observed increase in cross-sectional area of BLA neurons (Berdel *et al.* 1997*a*) and likely involve insertion of ion channels into the membrane. The developmental reduction of R_{in} would, in isolation, reduce responsiveness to synaptic input, and may serve as a homeostatic mechanism to compensate for increasing synaptic strength, as seen elsewhere (Zhang, 2004). The larger τ_{memb} in younger neurons means their voltage responses to synaptic input would be slower, promoting temporal summation of inputs. However, this would also reduce temporal precision of action potentials, meaning preadolescent amygdala neurons may be less able to coordinate action potentials and take advantage of temporal coding and spike timing-dependent plasticity.

Maturation of membrane potential oscillations and resonance

Passive membrane properties like τ_{memb} also help shape oscillatory properties of neurons, which influence the sensitivity of neurons to input and production of action potentials based on input frequency. Over the first postnatal month, the proportion of BLA principal neurons expressing spontaneous membrane potential oscillations (MPOs) increased substantially and the frequency of those MPOs increased. Spontaneous MPOs are expressed in adult BLA principal neurons in the guinea pig at a proportion comparable to that seen here at P21 and P28 (Pape *et al.* 1998). The change in frequency with development was not significant, although similar trends have been observed in entorhinal cortex (Boehlen *et al.* 2010) and midbrain (Wu *et al.* 2001). Interestingly, the MPO was abolished by application of 1 μM tetrodotoxin (authors' unpublished observation), suggesting the oscillation is promoted by synaptic activity.

Maturation of intrinsic oscillatory activity in BLA principal neurons also manifests as a change in the preferred resonance frequency. Intrinsic resonance has a similar time course of development to the MPO, expressing a mature phenotype in the BLA at P21. Resonance and MPOs also exhibit coordinated development in neurons of the entorhinal cortex (Burton *et al.* 2008; Boehlen *et al.* 2010). These two phenomena are mediated by a similar set of voltage-gated currents and have similar frequency preference (Lampl & Yarom, 1997; Hutcheon & Yarom, 2000; Erchova *et al.* 2004). The mean peak resonance frequency we report here for BLA principal neurons at P28, 5.69 Hz, differs substantially from those reported previously for the guinea pig, 2.5 Hz (Pape & Driesang, 1998), and the adult rat, 4.2 Hz (Ryan *et al.* 2012). While these differences could be due to continued maturation of oscillatory properties after P28, we believe it is more likely to be due to differences in species or recording voltage, which is known to impact resonance (Pape & Driesang, 1998; Tseng & Nadim, 2010).

Spontaneous MPOs can directly influence spike timing (Desmaisons *et al.* 1999; Richardson *et al.* 2003), and in our hands, action potentials were phase-locked with the peak of the spontaneous MPO in some neurons at P28. Oscillatory properties of individual neurons contribute to the production of network oscillations (Lampl & Yarom, 1997; Tohidi & Nadim, 2009), which are an important component of communication between distant brain regions (Engel *et al.* 2001; Singer, 2009; Canolty & Knight, 2010; Fujisawa & Buzsaki, 2011). Coherent oscillations are expressed by the amygdala and downstream target regions, including the hippocampus and prefrontal cortex, during fear acquisition and expression (Madsen & Rainnie, 2009; Sangha *et al.* 2009; Pape & Pare, 2010). Importantly, the frequency of these coherent oscillations overlaps with the frequency of peak resonance and spontaneous MPOs in BLA principal neurons at P28, suggesting the emergence of these properties contributes to the mature expression of fear. Theta oscillations in local field potentials from the hippocampus increase in frequency throughout the third and fourth postnatal weeks, corresponding with emergence of mature network properties (Wills *et al.* 2010). This finding further supports a role for development of the oscillatory properties of individual neurons in network function and mature behaviour.

Considering the importance of oscillatory properties of individual neurons for the generation of network oscillations (Lampl & Yarom, 1997; Desmaisons *et al.* 1999; Richardson *et al.* 2003; Tohidi & Nadim, 2009), their emergence in the BLA should correspond with that of principal neuron resonance. Based on electroencephalograms of the developing rat brain, no discernible network oscillations are observed in the BLA from birth through P14. Prominent oscillations emerge by this age in other regions including cortex, hippocampus and thalamus (Snead & Stephens, 1983), suggesting network oscillations in the BLA develop relatively late. We have recently argued that network oscillations in the amygdala are promoted by organization of principal neuron MPOs by synaptic input from parvalbumin-expressing interneurons (Ryan *et al.* 2012). Interestingly, these interneurons emerge in the BLA at P14 and reach mature expression by P21 (Berdel & Morys, 2000), when

mature oscillatory properties would render BLA principal neurons more susceptible to organization by parvalbumin interneurons.

Maturation of I_h and its contribution to resonance

The observed changes to resonance, as well as to passive membrane properties, were likely to be influenced by maturation of the voltage-sensitive current, I_h. This current is critically involved in the expression of resonance properties (Hutcheon *et al.* 1996; Hu *et al.* 2002; Marcelin *et al.* 2012) and contributes to input resistance at rest (Surges *et al.* 2004). Here we have shown an increase in amplitude and a decrease in activation time constant of I_h across the first postnatal month, as shown previously in other brain regions (Vasilyev & Barish, 2002; Khurana *et al.* 2012). The interaction of a sevenfold increase in I_h current amplitude across this window with a nearly 10-fold reduction of R_{in} explains the fairly consistent amplitude of voltage sag at all ages. A consistent sag amplitude across the first postnatal month was also observed in entorhinal cortex despite increasing I_h conductance (Burton *et al.* 2008). The amplitude of I_h may be regulated throughout the first postnatal month to homeostatically maintain a consistent resting membrane potential. There are, however, visible changes in the voltage waveform of I_h because of faster I_h activation and τ_{memb}. We have preliminary evidence suggesting the changes in I_h are due to transitions in the expression of subtypes of HCN, the channel mediating I_h, in BLA principal neurons (Ehrlich *et al.* 2010), similar to in thalamic and hippocampal neurons (Bender *et al.* 2001; Kanyshkova *et al.* 2009). I_h activation kinetics were assessed by fitting the Cs^+ subtraction current with a two-term exponential equation at P14, P21 and P28, since I_h has previously been shown to have two distinct activation time constants (Pena *et al.* 2006). It is not clear why I_h at P7 appeared to have only a single activation time constant. While Cs^+ is not selective for HCN channels, we believe the subtraction currents are largely composed of I_h. The hyperpolarization-activated current we observed is likely to have involved activation of voltage-gated K^+ channels, which can also be sensitive to Cs^+. However, for Cs^+ to affect those channels, it must enter the cell, which is unlikely at the voltages used for this protocol. Assessed by blockade with Cs^+, I_h makes a substantial contribution to resonance as early as P14. From P14 to P28, Cs^+ shifted the peak resonance toward lower frequencies, but at P7 there was little impact. Interestingly, the greatest effects on resonance of I_h blockade were seen at P14, when the resonance in Cs^+ resembled that seen at P7 in control conditions. This suggests I_h emerges as a major contributor to resonance between P7 and P14. Starting at P21, Cs^+ did not functionally abolish resonance by enhancing power preferentially in the lowest frequencies, as it did at P14. Cs^+ application had a diminishing effect on resonance with age following P14, suggesting other currents begin to play a greater role in shaping resonance. Considering the unique role I_h plays in shaping resonance at P14, at that age we expect profound sensitivity of resonance to neuromodulators that influence cAMP, a classic modulator of I_h. Developmental changes in neuromodulators contribute to maturation of I_h around P14 in the medial superior olive, further suggesting neuromodulation is relevant for neuronal function at that age (Khurana *et al.* 2012). Interestingly, I_h conductance in BLA principal neurons is reduced by the anxiolytic neurotransmitter neuropeptide Y and enhanced by the anxiogenic neurotransmitter corticotrophin-releasing factor (Giesbrecht *et al.* 2010).

Changes to resonance due to blockade of I_h are indirect and largely attributable to effects on τ_{memb}. There is a close relationship between τ_{memb} and peak resonance frequency (Hutcheon & Yarom, 2000), and the magnitude of resonance is linearly correlated with I_h amplitude (Marcelin *et al.* 2012). We showed that blockade of I_h directly impacts τ_{memb} but does not maintain the fitted relationship between τ_{memb} and peak resonance frequency, suggesting that, aside from passively contributing to resonance through τ_{memb}, I_h contributes actively through its voltage dependence and activation kinetics. In hippocampal pyramidal neurons, the amplitude of I_h is tightly correlated with the magnitude of the resonance peak (Marcelin *et al.* 2012).

Maturation of trains of action potentials

As expected, trains of action potentials elicited by direct current injection changed qualitatively across the first postnatal month. At P7, neurons exhibited a consistent action potential frequency throughout trains; as the animals aged, the frequency of the first two to three spikes increased dramatically, such that mature cells exhibited doublets or triplets at the onset of firing. Spike doublets have been documented in adult neurons of the basolateral (Rainnie *et al.* 1993) and lateral (Driesang & Pape, 2000) nuclei of the amygdala, and are thought to improve the fidelity of synaptic transmission (Lisman, 1997). Furthermore, doublets have been suggested to promote network oscillations and bridge the temporal gap between inputs to the amygdala representing conditioned and unconditioned stimuli during fear conditioning (Driesang & Pape, 2000). Interestingly, changes in dendritic morphology can directly affect spiking properties, including doublet firing (Mainen & Sejnowski, 1996), and experiments are underway to characterize morphological changes in these neurons during development.

In this study, maximal firing rate reached maturity in P14 cells, while in cortical pyramidal neurons, maximal firing rates have been reported to reach mature values

as early as P2 (McCormick & Prince, 1987). This disparity is consistent with the late development of emotional processing relative to sensorimotor processing. The consistency of firing rates after P14 may be afforded by strengthening of I_A through insertion of Kv4 channels into the membrane (Vacher *et al.* 2006) to compensate for reduced medium afterhyperpolarizations (mAHPs).

It is important to note that, while spike trains elicited with square current pulses were relatively consistent across the first postnatal month, there were profound changes in the spontaneous activity of neurons depolarized to near threshold with direct current. Specifically, neurons at P7 exhibited highly erratic membrane potentials characterized by waves of depolarization, likely involving activation of low-threshold calcium currents, which resulted in bursts of action potentials and periods of quiescence. Throughout the first postnatal month, membrane potentials became more stable near threshold. It is possible that the erratic membrane potentials in immature neurons were due to instability of the seal or physical qualities of the membrane. This is likely not to be the case based on the high R_{in} and repetitive firing exhibited at P7, properties indicative of a healthy membrane and seal. Furthermore, the membrane potential at P7 was stabilized by application of TTX (authors' unpublished observation), suggesting the volatility was introduced by synaptic or intrinsic currents.

Maturation of action potentials and AHPs

There were also many developmental changes to properties of individual action potentials, including threshold, kinetics, and AHPs. Action potential threshold hyperpolarized until P21, potentially counteracting the effects of reduced R_{in} on neuronal excitability and acting to maintain consistent firing activity. The value we report for mature threshold (−41 mV) differed from the threshold values previously reported for mature BLA principal neurons (mean of −52 mV, (Rainnie *et al.* 1993), but this difference may be due to methods of recording (whole-cell patch *vs.* sharp) or analysis. Action potentials' rise time, decay time and half-width were halved from P7 to P28, with the majority of change occurring by P21. Thalamic neurons also achieve mature action potential durations around P21 (Ramoa & McCormick, 1994), while neocortical projection neurons do so somewhat earlier, at approximately P14 (McCormick & Prince, 1987). Faster action potentials would allow for faster firing rates and may also impact calcium influx due to spiking, which could impact AHPs of action potentials.

Across the first postnatal month, AHPs matured in two ways: mAHPs became significantly faster and shallower while fast AHPs (fAHPs) became faster and deeper. Fast AHPs were not present at P7 but were present in two-thirds of neurons by P21, when they exhibited adult-like waveforms. The emergence of fAHPs corresponds with faster action potential repolarization, and both of these phenomena are likely due to maturation of fast voltage-gated potassium currents. A reduction in mAHP duration across the first postnatal month has also been observed in entorhinal cortex (Burton *et al.* 2008). Medium AHPs can normalize inter-spike intervals and promote regular firing, hindering temporal coding mechanisms in favour of rate coding (Prescott & Sejnowski, 2008); smaller mAHPs in adult principal neurons are therefore another factor, along with smaller τ_{memb} and more prominent oscillations, which could promote temporal coding in mature emotional processing. Both fAHPs and mAHPs have been reported in adult BLA principal neurons (Rainnie *et al.* 1993), and the reported values suggest the trends we observed in AHP amplitude and duration continue past P28. A subset of adult BLA principal neurons has been shown to also express a slow AHP (Rainnie *et al.* 1993; Faber & Sah, 2002). Unfortunately, we were unable to assess the presence of a sAHP in immature BLA principal neurons with our data set. Future studies should address whether the presence of a sAHP emerges during postnatal development, as this could shed light on the developmental differentiation of principal neuron subtypes.

The trajectory of fAHP maturation corresponds with a reduction of the first inter-spike interval, such that almost all neurons at P28 have a fAHP and fire doublets. Interestingly, reduction of fAHP amplitude in the lateral amygdala through modulation of BK channels has been shown following stress and linked to anxiety (Guo *et al.* 2012), suggesting doublets are relevant for amygdala function. While the emergence of a fAHP likely involves changes in currents like BK, we cannot make any direct claims regarding the quantity or quality of underlying currents because we measured voltage deflections. Furthermore, because these voltage deflections are measured relative to action potential threshold, which is itself changing across development, the interaction of AHPs with currents regulating inter-spike interval may vary with age.

Maturation of amygdala morphology and connectivity

Although this is the first study characterizing the maturation of amygdala physiology, several studies have addressed other aspects of amygdala development. The basolateral complex of the rat amygdala emerges by embryonic day (E)17 (Berdel *et al.* 1997*b*), with the majority of neurogenesis occurring between E14 and E16 (Bayer *et al.* 1993). The BLA continues to increase in volume until P14 (Berdel *et al.* 1997*b*), although the total number of neurons reaches the mature value at P7.

Interestingly, in terms of BLA volume and number of neurons, throughout development no differences were observed across sex (Rubinow & Juraska, 2009); this corroborates our findings of no sex differences in principal neuron physiology. From birth to P7, the cross-sectional area of rat BLA neurons doubles, but at P7 the majority of neurons are still small and have only one or two main dendrites (Berdel *et al.* 1997*a*). By P14, the cross-sectional area is the same as in the adult. A threefold increase in total synapse in the BLA from P7 to P28, as measured by synaptophysin staining (Morys *et al.* 1998), probably reflects increased intrinsic connectivity as well as maturation of inputs to the amygdala.

The BLA contributes to a network of brain regions that produce and regulate emotional behaviour, including the prefrontal cortex, which itself develops substantially during the first postnatal month (Van Eden & Uylings, 1985; Bourgeois *et al.* 1994; Anderson *et al.* 1995; Rakic, 1995; Gourley *et al.* 2012). Afferents from cortical areas, including the prefrontal and auditory cortices, do not emerge in the BLA until around P13, while thalamic afferents are present as early as P7 (Bouwmeester *et al.* 2002). Interestingly, a functional interaction of the prefrontal cortex and BLA also develops late; the medial prefrontal cortex does not contribute to extinction learning until P24 (Kim *et al.* 2009).

We have provided evidence that neurons of the BLA are not physiologically mature at birth, and have argued that postnatal changes in amygdala function and emotional processing are likely to be driven by drastic changes to the physiology of amygdala neurons. In light of these findings, future studies should address the maturation of ionic currents in BLA principal neurons and how their development contributes to the physiological changes we observed. We predict that changes to excitatory and inhibitory synaptic transmission occur in concert with the observed maturation of intrinsic neurophysiology; understanding the interaction of these processes will be critical in determining the excitability of the immature amygdala and the patterning of its activity. This may help us understand the ontogeny of amygdala network oscillations and, in turn, how changes in their robustness or frequency contribute to the development of fear learning. Finally, to better understand the aetiology of psychiatric disorders with developmental underpinnings, future studies should characterize the developmental trajectory of amygdala neurons in the face of perturbations such as early-life stress, teratogens and genetic predispositions for psychiatric illness.

References

Adolphs R, Baron-Cohen S & Tranel D (2002). Impaired recognition of social emotions following amygdala damage. *J Cogn Neurosci* **14**, 1264–1274.

Anderson SA, Classey JD, Conde F, Lund JS & Lewis DA (1995). Synchronous development of pyramidal neuron dendritic spines and parvalbumin-immunoreactive chandelier neuron axon terminals in layer III of monkey prefrontal cortex. *Neuroscience* **67**, 7–22.

Bayer SA, Altman J, Russo RJ & Zhang X (1993). Timetables of neurogenesis in the human brain based on experimentally determined patterns in the rat. *Neurotoxicology* **14**, 83–144.

Bender RA, Brewster A, Santoro B, Ludwig A, Hofmann F, Biel M & Baram TZ (2001). Differential and age-dependent expression of hyperpolarization-activated, cyclic nucleotide-gated cation channel isoforms 1–4 suggests evolving roles in the developing rat hippocampus. *Neuroscience* **106**, 689–698.

Berdel B & Morys J (2000). Expression of calbindin-D28k and parvalbumin during development of rat's basolateral amygdaloid complex. *Int J Dev Neurosci* **18**, 501–513.

Berdel B, Morys J & Maciejewska B (1997*a*). Neuronal changes in the basolateral complex during development of the amygdala of the rat. *Int J Dev Neurosci* **15**, 755–765.

Berdel B, Morys J, Maciejewska B & Dziewiatkowski J (1997b). Volume and topographical changes of the basolateral complex during the development of the rat's amygdaloid body. *Folia Morphol* **56**, 1–11.

Boehlen A, Heinemann U & Erchova I (2010). The range of intrinsic frequencies represented by medial entorhinal cortex stellate cells extends with age. *J Neurosci* **30**, 4585–4589.

Bokil H, Andrews P, Kulkarni JE, Mehta S & Mitra PP (2010). Chronux: a platform for analyzing neural signals. *J Neurosci Methods* **192**, 146–151.

Bourgeois JP, Goldman-Rakic PS & Rakic P (1994). Synaptogenesis in the prefrontal cortex of rhesus monkeys. *Cereb Cortex* **4**, 78–96.

Bouwmeester H, Smits K & Van Ree JM (2002). Neonatal development of projections to the basolateral amygdala from prefrontal and thalamic structures in rat. *J Comp Neurol* **450**, 241–255.

Brummelte S, Witte V & Teuchert-Noodt G (2007). Postnatal development of GABA and calbindin cells and fibers in the prefrontal cortex and basolateral amygdala of gerbils (*Meriones unguiculatus*). *Int J Dev Neurosci* **25**, 191–200.

Burton BG, Economo MN, Lee GJ & White JA (2008). Development of theta rhythmicity in entorhinal stellate cells of the juvenile rat. *J Neurophysiol* **100**, 3144–3157.

Campbell BA & Ampuero MX (1985). Dissociation of autonomic and behavioral components of conditioned fear during development in the rat. *Behav Neurosci* **99**, 1089–1102.

Canolty RT & Knight RT (2010). The functional role of cross-frequency coupling. *Trends Cogn Sci* **14**, 506–515.

Cohen J (1977). *Statistical Power Analysis for the Behavioral Sciences*. Academic Press, New York.

Davila JC, Olmos L, Legaz I, Medina L, Guirado S & Real MA (2008). Dynamic patterns of colocalization of calbindin, parvalbumin and GABA in subpopulations of mouse basolateral amygdalar cells during development. *J Chem Neuroanat* **35**, 67–76.

Davis M (2000). The role of the amygdala in conditioned and unconditioned fear and anxiety. In *The Amygdala: A Functional Analysis*, ed. Aggleton JP, pp. 255–305. Oxford University Press, Oxford.

Davis M, Walker DL & Myers KM (2003). Role of the amygdala in fear extinction measured with potentiated startle. *Ann N Y Acad Sci* **985**, 218–232.

Desmaisons D, Vincent JD & Lledo PM (1999). Control of action potential timing by intrinsic subthreshold oscillations in olfactory bulb output neurons. *J Neurosci* **19**, 10727–10737.

Driesang RB & Pape HC (2000). Spike doublets in neurons of the lateral amygdala: mechanisms and contribution to rhythmic activity. *Neuroreport* **11**, 1703–1708.

Ehrlich DE, Ryan SJ, Hazra R, Guo JD & Rainnie DG (2010). Postnatal development of I(h) subunit expression contributes to maturation of intrinsic resonance properties in principal neurons of the basolateral amygdala. *2010 Abstract Viewer/Itinerary Planner*, Programme No. 885.3. Society for Neuroscience, Washington, DC.

Ehrlich I, Humeau Y, Grenier F, Ciocchi S, Herry C & Luthi A (2009). Amygdala inhibitory circuits and the control of fear memory. *Neuron* **62**, 757–771.

Engel AK, Fries P & Singer W (2001). Dynamic predictions: oscillations and synchrony in top-down processing. *Nat Rev Neurosci* **2**, 704–716.

Erchova I, Kreck G, Heinemann U & Herz AV (2004). Dynamics of rat entorhinal cortex layer II and III cells: characteristics of membrane potential resonance at rest predict oscillation properties near threshold. *J Physiol* **560**, 89–110.

Erdfelder E, Faul F & Buchner A (1996). GPOWER: A general power analysis program. *Behav Res Methods* **28**, 1–11.

Faber ES & Sah P (2002). Physiological role of calcium-activated potassium currents in the rat lateral amygdala. *J Neurosci* **22**, 1618–1628.

Fujisawa S & Buzsaki G (2011). A 4 Hz oscillation adaptively synchronizes prefrontal, VTA, and hippocampal activities. *Neuron* **72**, 153–165.

Giesbrecht CJ, Mackay JP, Silveira HB, Urban JH & Colmers WF (2010). Countervailing modulation of Ih by neuropeptide Y and corticotrophin-releasing factor in basolateral amygdala as a possible mechanism for their effects on stress-related behaviors. *J Neurosci* **30**, 16970–16982.

Gourley SL, Olevska A, Warren MS, Taylor JR & Koleske AJ (2012). Arg kinase regulates prefrontal dendritic spine refinement and cocaine-induced plasticity. *J Neurosci* **32**, 2314–2323.

Guo YY, Liu SB, Cui GB, Ma L, Feng B, Xing JH, Yang Q, Li XQ, Wu YM, Xiong LZ, Zhang W & Zhao MG (2012). Acute stress induces down-regulation of large-conductance Ca^{2+}-activated potassium channels in the lateral amygdala. *J Physiol* **590**, 875–886.

Gutfreund Y, Yarom Y & Segev I (1995). Subthreshold oscillations and resonant frequency in guinea-pig cortical neurons: physiology and modelling. *J Physiol* **483**, 621–640.

Hazra R, Guo JD, Ryan SJ, Jasnow AM, Dabrowska J, Rainnie DG (2011). A transcriptomic analysis of type I-III neurons in the bed nucleus of the stria terminalis. *Mol Cell Neurosci.* **46**, 699–709.

Heim C & Nemeroff CB (2002). Neurobiology of early life stress: clinical studies. *Semin Clin Neuropsychiatry* **7**, 147–159.

Hicks BM, DiRago AC, Iacono WG & McGue M (2009). Gene-environment interplay in internalizing disorders: consistent findings across six environmental risk factors. *J Child Psychol Psychiatry* **50**, 1309–1317.

Hu H, Vervaeke K & Storm JF (2002). Two forms of electrical resonance at theta frequencies, generated by M-current, h-current and persistent Na^+ current in rat hippocampal pyramidal cells. *J Physiol* **545**, 783–805.

Hunt PS, Richardson R & Campbell BA (1994). Delayed development of fear-potentiated startle in rats. *Behav Neurosci* **108**, 69–80.

Hutcheon B, Miura RM & Puil E (1996). Models of subthreshold membrane resonance in neocortical neurons. *J Neurophysiol* **76**, 698–714.

Hutcheon B & Yarom Y (2000). Resonance, oscillation and the intrinsic frequency preferences of neurons. *Trends Neurosci* **23**, 216–222.

Izhikevich EM (2002). Resonance and selective communication via bursts in neurons having subthreshold oscillations. *Biosystems* **67**, 95–102.

Kanyshkova T, Pawlowski M, Meuth P, Dube C, Bender RA, Brewster AL, Baumann A, Baram TZ, Pape HC & Budde T (2009). Postnatal expression pattern of HCN channel isoforms in thalamic neurons: relationship to maturation of thalamocortical oscillations. *J Neurosci* **29**, 8847–8857.

Kessler RC, Berglund P, Demler O, Jin R, Merikangas KR & Walters EE (2005). Lifetime prevalence and age-of-onset distributions of DSM-IV disorders in the National Comorbidity Survey Replication. *Arch Gen Psychiatry* **62**, 593–602.

Khurana S, Liu Z, Lewis AS, Rosa K, Chetkovich D & Golding NL (2012). An essential role for modulation of hyperpolarization-activated current in the development of binaural temporal precision. *J Neurosci* **32**, 2814–2823.

Kim-Cohen J, Caspi A, Moffitt TE, Harrington H, Milne BJ & Poulton R (2003). Prior juvenile diagnoses in adults with mental disorder: developmental follow-back of a prospective-longitudinal cohort. *Arch Gen Psychiatry* **60**, 709–717.

Kim JH, Hamlin AS & Richardson R (2009). Fear extinction across development: the involvement of the medial prefrontal cortex as assessed by temporary inactivation and immunohistochemistry. *J Neurosci* **29**, 10802–10808.

Kim JH & Richardson R (2007). A developmental dissociation in reinstatement of an extinguished fear response in rats. *Neurobiol Learn Mem* **88**, 48–57.

Koob GF & Volkow ND (2010). Neurocircuitry of addiction. *Neuropsychopharmacology* **35**, 217–238.

Kraszpulski M, Dickerson PA & Salm AK (2006). Prenatal stress affects the developmental trajectory of the rat amygdala. *Stress* **9**, 85–95.

Lampl I & Yarom Y (1997). Subthreshold oscillations and resonant behavior: two manifestations of the same mechanism. *Neuroscience* **78**, 325–341.

LeDoux J (2000). The amygdala and emotion: a view through fear. In *The Amygdala: A Functional Analysis*, ed. Aggleton JP, pp. 339–351. Oxford University Press, Oxford.

LeDoux J (2007). The amygdala. *Curr Biol* **17**, R868–874.

Lesting J, Narayanan RT, Kluge C, Sangha S, Seidenbecher T & Pape HC (2011). Patterns of coupled theta activity in amygdala-hippocampal-prefrontal cortical circuits during fear extinction. *PloS One* **6**, e21714.

Lisman JE (1997). Bursts as a unit of neural information: making unreliable synapses reliable. *Trends Neurosci* **20**, 38–43.

Llinas RR, Grace AA & Yarom Y (1991). In vitro neurons in mammalian cortical layer 4 exhibit intrinsic oscillatory activity in the 10- to 50-Hz frequency range. *Proc Natl Acad Sci U S A* **88**, 897–901.

Madsen TE & Rainnie DG (2009). Local field potentials in the rat basolateral amygdala and medial prefrontal cortex show coherent oscillations in multiple frequency bands during fear. *2009 Abstract Viewer/Itinerary Planner*, Programme No. 132.4. Society for Neuroscience, Washington, DC.

Mainen ZF & Sejnowski TJ (1996). Influence of dendritic structure on firing pattern in model neocortical neurons. *Nature* **382**, 363–366.

Marcelin B, Liu Z, Chen Y, Lewis AS, Becker A, McClelland S, Chetkovich DM, Migliore M, Baram TZ, Esclapez M & Bernard C (2012). Dorsoventral differences in intrinsic properties in developing CA1 pyramidal cells. *J Neurosci* **32**, 3736–3747.

McCormick DA & Prince DA (1987). Post-natal development of electrophysiological properties of rat cerebral cortical pyramidal neurones. *J Physiol* **393**, 743–762.

McDonald AJ (1985). Immunohistochemical identification of gamma-aminobutyric acid-containing neurons in the rat basolateral amygdala. *Neurosci Lett* **53**, 203–207.

McDonald AJ (1998). Cortical pathways to the mammalian amygdala. *Prog Neurobiol* **55**, 257–332.

McDonald AJ, Beitz AJ, Larson AA, Kuriyama R, Sellitto C & Madl JE (1989). Co-localization of glutamate and tubulin in putative excitatory neurons of the hippocampus and amygdala: an immunohistochemical study using monoclonal antibodies. *Neuroscience* **30**, 405–421.

McEwen BS (2003). Early life influences on life-long patterns of behavior and health. *Ment Retard Dev Disabil Res Rev* **9**, 149–154.

Monk CS (2008). The development of emotion-related neural circuitry in health and psychopathology. *Dev Psychopathol* **20**, 1231–1250.

Morys J, Berdel B, Kowianski P & Dziewiatkowski J (1998). The pattern of synaptophysin changes during the maturation of the amygdaloid body and hippocampal hilus in the rat. *Folia Neuropathol* **36**, 15–23.

Moye TB & Rudy JW (1987). Ontogenesis of trace conditioning in young rats: dissociation of associative and memory processes. *Dev Psychobiol* **20**, 405–414.

Pape HC & Driesang RB (1998). Ionic mechanisms of intrinsic oscillations in neurons of the basolateral amygdaloid complex. *J Neurophysiol* **79**, 217–226.

Pape HC & Pare D (2010). Plastic synaptic networks of the amygdala for the acquisition, expression, and extinction of conditioned fear. *Physiol Rev* **90**, 419–463.

Pape HC, Pare D & Driesang RB (1998). Two types of intrinsic oscillations in neurons of the lateral and basolateral nuclei of the amygdala. *J Neurophysiol* **79**, 205–216.

Pena F, Amuzescu B, Neaga E & Flonta ML (2006). Thermodynamic properties of hyperpolarization-activated current (Ih) in a subgroup of primary sensory neurons. *Exp Brain Res* **173**, 282–290.

Pine DS (2002). Brain development and the onset of mood disorders. *Semin Clin Neuropsychiatry* **7**, 223–233.

Pine DS, Cohen P, Gurley D, Brook J & Ma Y (1998). The risk for early-adulthood anxiety and depressive disorders in adolescents with anxiety and depressive disorders. *Arch Gen Psychiatry* **55**, 56–64.

Popa D, Duvarci S, Popescu AT, Lena C & Pare D (2010). Coherent amygdalocortical theta promotes fear memory consolidation during paradoxical sleep. *Proc Natl Acad Sci U S A* **107**, 6516–6519.

Prescott SA & Sejnowski TJ (2008). Spike-rate coding and spike-time coding are affected oppositely by different adaptation mechanisms. *J Neurosci* **28**, 13649–13661.

Quinn R (2005). Comparing rat's to human's age: How old is my rat in people years? *Nutrition* **21**, 775–777.

Rainnie DG (1999). Serotonergic modulation of neurotransmission in the rat basolateral amygdala. *J Neurophysiol* **82**, 69–85.

Rainnie DG, Asprodini EK & Shinnick-Gallagher P (1991*a*). Excitatory transmission in the basolateral amygdala. *J Neurophysiol* **66**, 986–998.

Rainnie DG, Asprodini EK & Shinnick-Gallagher P (1991*b*). Inhibitory transmission in the basolateral amygdala. *J Neurophysiol* **66**, 999–1009.

Rainnie DG, Asprodini EK & Shinnick-Gallagher P (1993). Intracellular recordings from morphologically identified neurons of the basolateral amygdala. *J Neurophysiol* **69**, 1350–1362.

Rainnie DG, Bergeron R, Sajdyk TJ, Patil M, Gehlert DR & Shekhar A (2004). Corticotrophin releasing factor-induced synaptic plasticity in the amygdala translates stress into emotional disorders. *J Neurosci* **24**, 3471–3479.

Rakic P (1995). The development of the frontal lobe. A view from the rear of the brain. *Adv Neurol* **66**, 1–6; discussion 6–8.

Ramoa AS & McCormick DA (1994). Developmental changes in electrophysiological properties of LGNd neurons during reorganization of retinogeniculate connections. *J Neurosci* **14**, 2089–2097.

Richardson MJ, Brunel N & Hakim V (2003). From subthreshold to firing-rate resonance. *J Neurophysiol* **89**, 2538–2554.

Richardson R, Paxinos G & Lee J (2000). The ontogeny of conditioned odor potentiation of startle. *Behav Neurosci* **114**, 1167–1173.

Rubinow MJ & Juraska JM (2009). Neuron and glia numbers in the basolateral nucleus of the amygdala from preweaning through old age in male and female rats: a stereological study. *J Comp Neurol* **512**, 717–725.

Ryan SJ, Ehrlich DE, Jasnow AJ, Daftary S, Madsen TE & Rainnie DG (2012). Spike-timing precision and neuronal synchrony are enhanced by an interaction between synaptic inhibition and membrane oscillations in the amygdala. *PloS One* **7**, e35320.

Sadler TR, Nguyen PT, Yang J, Givrad TK, Mayer EA, Maarek JM, Hinton DR & Holschneider DP (2011). Antenatal maternal stress alters functional brain responses in adult offspring during conditioned fear. *Brain Res* **1385**, 163–174.

Sancristobal B, Sancho JM & Garcia-Ojalvo J (2010). Phase-response approach to firing-rate selectivity in neurons with subthreshold oscillations. *Phys Rev E Stat Nonlin Soft Matter Phys* **82**, 041908.

Sangha S, Narayanan RT, Bergado-Acosta JR, Stork O, Seidenbecher T & Pape HC (2009). Deficiency of the 65 kDa isoform of glutamic acid decarboxylase impairs extinction of cued but not contextual fear memory. *J Neurosci* **29**, 15713–15720.

Seidel K, Helmeke C, Poeggel G & Braun K (2008). Repeated neonatal separation stress alters the composition of neurochemically characterized interneuron subpopulations in the rodent dentate gyrus and basolateral amygdala. *Dev Neurobiol* **68**, 1137–1152.

Shekhar A, Truitt W, Rainnie D & Sajdyk T (2005). Role of stress, corticotrophin releasing factor (CRF) and amygdala plasticity in chronic anxiety. *Stress* **8**, 209–219.

Singer W (2009). Distributed processing and temporal codes in neuronal networks. *Cogn Neurodyn* **3**, 189–196.

Snead OC 3rd & Stephens HI (1983). Ontogeny of cortical and subcortical electroencephalographic events in unrestrained neonatal and infant rats. *Exp Neuro* **82**, 249–269.

Spear LP (2009). Heightened stress responsivity and emotional reactivity during pubertal maturation: Implications for psychopathology. *Dev Psychopathol* **21**, 87–97.

Steinberg L (2005). Cognitive and affective development in adolescence. *Trends Cogn Sci* **9**, 69–74.

Storm JF (1989). An after-hyperpolarization of medium duration in rat hippocampal pyramidal cells. *J Physiol* **409**, 171–190.

Sullivan RM, Landers M, Yeaman B & Wilson DA (2000). Good memories of bad events in infancy. *Nature* **407**, 38–39.

Surges R, Freiman TM & Feuerstein TJ (2004). Input resistance is voltage dependent due to activation of Ih channels in rat CA1 pyramidal cells. *J Neurosci Res* **76**, 475–480.

Tohidi V & Nadim F (2009). Membrane resonance in bursting pacemaker neurons of an oscillatory network is correlated with network frequency. *J Neurosci* **29**, 6427–6435.

Truitt WA, Sajdyk TJ, Dietrich AD, Oberlin B, McDougle CJ & Shekhar A (2007). From anxiety to autism: spectrum of abnormal social behaviors modeled by progressive disruption of inhibitory neuronal function in the basolateral amygdala in Wistar rats. *Psychopharmacology* **191**, 107–118.

Tseng HA & Nadim F (2010). The membrane potential waveform of bursting pacemaker neurons is a predictor of their preferred frequency and the network cycle frequency. *J Neurosci* **30**, 10809–10819.

Vacher H, Diochot S, Bougis PE, Martin-Eauclaire MF & Mourre C (2006). Kv4 channels sensitive to BmTX3 in rat nervous system: autoradiographic analysis of their distribution during brain ontogenesis. *Eur J Neurosci* **24**, 1325–1340.

Van Eden CG & Uylings HB (1985). Postnatal volumetric development of the prefrontal cortex in the rat. *J Comp Neurol* **241**, 268–274.

Vasilyev DV & Barish ME (2002). Postnatal development of the hyperpolarization-activated excitatory current Ih in mouse hippocampal pyramidal neurons. *J Neurosci* **22**, 8992–9004.

Wills TJ, Cacucci F, Burgess N & O'Keefe J (2010). Development of the hippocampal cognitive map in preweanling rats. *Science* **328**, 1573–1576.

Wu N, Hsiao CF & Chandler SH (2001). Membrane resonance and subthreshold membrane oscillations in mesencephalic V neurons: participants in burst generation. *J Neurosci* **21**, 3729–3739.

Zhang TY, Parent C, Weaver I & Meaney MJ (2004). Maternal programming of individual differences in defensive responses in the rat. *Ann N Y Acad Sci* **1032**, 85–103.

Zhang ZW (2004). Maturation of layer V pyramidal neurons in the rat prefrontal cortex: intrinsic properties and synaptic function. *J Neurophysiol* **91**, 1171–1182.

Author contributions

These experiments were performed in the laboratory of D.G.R. D.E.E. and S.J.R. contributed to the conception and design of experiments, collected, analysed, and interpreted data, and drafted and revised the manuscript. D.G.R. contributed to the conception and design of experiments, interpreted data, and revised the manuscript. All authors approved the final version of the manuscript.

Acknowledgements

We would like to thank Professor Shannon L. Gourley for her constructive comments on the manuscript. We would also like to thank the National Institutes of Health (Grants MH 069852 to D.G.R., base grant RR 00165 to the Yerkes National Primate Research centre, and MH 090729 to D.E.E.) for funding.